Retrieval of the raindrop size distribution from polarimetric radar data using double-moment normalisation

Timothy H. Raupach and Alexis Berne

Environmental Remote Sensing Laboratory, School of Architecture, Civil, and Environmental Engineering, École Polytechnique Fédérale de Lausanne (EPFL), 1015 Lausanne, Switzerland

Correspondence to: Alexis Berne (alexis.berne@epfl.ch)

Abstract. A new technique for estimating the raindrop size distribution (DSD) from polarimetric radar data is proposed. Two statistical moments of the DSD are estimated from polarimetric variables, and the DSD is reconstructed using a double-moment normalisation. The technique takes advantage of the relative invariance of the double-moment normalised DSD. The method was tested using X-band radar data and networks of disdrometers in three different climatic regions. Radar-derived estimates of the DSD compare reasonably well to observations. In the three tested domains, the proposed method performs similarly to and often better than a state-of-the-art DSD-retrieval technique. The approach is flexible because no specific DSD model is prescribed. In addition, a method is proposed to treat noisy radar data to improve DSD-retrieval performance with radar measurements.

1 Introduction

The raindrop size distribution (DSD) describes the microstructure of liquid precipitation, and is highly variable (Jameson and Kostinski, 2001; Uijlenhoet et al., 2003; Tapiador et al., 2010; Jaffrain and Berne, 2012). The DSD is measured at the point scale by disdrometers. For applications such as numerical weather prediction (e.g. Baldauf et al., 2011) or radar remote sensing (e.g. Bringi and Chandrasekar, 2001) it is often necessary to know the areal DSD at the pixel scale. In other cases, such as studies of the microphysics of precipitation (Pruppacher and Klett, 2000; Tapiador et al., 2014), it would be useful to be able to remotely infer the DSD aloft or in remote locations. For these reasons, retrieval of the DSD from radar data has been a long-standing goal. In this paper we present a new technique for DSD retrieval from polarimetric radar data, which is based on the double-moment normalisation technique of Lee et al. (2004).

Polarimetric weather radars are particularly useful for remote retrieval of the DSD, because differences between vertically and horizontally polarised electromagnetic waves reflected off hydrometeors in the atmosphere provide information on the particles' concentration, size, and shape. In rainfall, radar reflectivity in horizontal (Z_H [dBZ]) or vertical (Z_V [dBZ]) polarisation primarily relates to drop concentration and size, differential reflectivity (Z_{DR} [dB]) reflects drop shape, and specific differential phase shift on propagation (K_{dp} [$^\circ$ km^{-1}]) relates to both the concentration and shape of the drops (Bringi and Chandrasekar, 2001). Seliga and Bringi (1976) showed that Z_{DR} can be linked to the median volume drop diameter, a microphysical property of rain. Since then, many methods for DSD retrieval from radar variables have been proposed.

Zhang et al. (2001) introduced the "constrained gamma" method, in which the shape and slope parameters of a gamma DSD model (Ulbrich, 1983) are assumed dependent. This assumption is subject to debate (e.g. Zhang et al., 2003; Atlas and Ulbrich, 2006; Moisseev and Chandrasekar, 2007; Cao and Zhang, 2009). The technique, modified by Brandes et al. (2003), can provide useful DSD information (Brandes et al., 2004a). In the "beta" method (Gorgucci et al., 2002), the effective slope of the drop axis ratio to diameter relationship is retrieved. The slope is used to find parameter values for the normalised gamma model of Willis (1984), which has advantages for use with polarimetric observations (Illingworth and Blackman, 2002). Retrieval of the gamma model shape parameter with the beta method is subject to high uncertainty (Gorgucci et al., 2002; Anagnostou et al., 2008). To deal with noisy Z_{DR} and K_{dp} data at low rain rates, Bringi et al. (2002, 2003) used the beta method for heavy rain and disdrometer-based regressions on Z_H and Z_{DR} for light rain. Brandes et al. (2004b) found that the constrained gamma method was in better agreement with disdrometer data than the beta method, while Anagnostou et al. (2008) reported similar performance from the two techniques, and both studies noted that the beta method is sensitive to errors in K_{dp}. Vulpiani et al. (2006) developed a neural-network DSD-retrieval technique, and spatial correlations of DSD model parameters have been retrieved from radar data (Thurai et al., 2012; Bringi et al., 2015).

X-band polarimetric weather radars are popular due to their portability, small size, and high resolution and sensitivity, but measurements at X-band suffer from attenuation by heavy rain (Anagnostou et al., 2013; Kalogiros et al., 2013) and must be corrected (Matrosov et al., 2005; Park et al., 2005a). Several DSD-retrieval algorithms have been developed for X-band (e.g. Park et al., 2005b; Gorgucci et al., 2008; Anagnostou et al., 2013; Kalogiros et al., 2013), including some with integrated attenuation correction (e.g. Testud et al., 2000; Yoshikawa et al., 2014). The self-consistent with optional parameterization attenuation correction and microphysics estimation (SCOP-ME) algorithm, developed through studies by Anagnostou et al. (2009, 2010) and Kalogiros et al. (2013), uses relationships calculated for the Rayleigh limit, corrected for Mie scattering at X-band. It performs well compared to contemporary algorithms and disdrometer observations (Anagnostou et al., 2013). In this paper we present a new method for DSD retrieval that uses the double-moment DSD normalisation of Lee et al. (2004), and compare it to SCOP-ME.

The rest of this manuscript is organised as follows: we briefly describe the double-moment DSD normalisation technique of Lee et al. (2004) in Section 2. Bulk rainfall variables that we use are introduced in Section 3. Data used are presented in Section 4. In Section 5 we propose a new DSD-retrieval method that uses double-moment normalisation to retrieve the DSD from polarimetric radar data. Its performance is compared to that of SCOP-ME using radar variables simulated from DSD measurements in Section 6. In Section 7 we introduce a new method to reduce the effects of noise in radar measurements. Using this method, the DSD-retrieval algorithms are compared using radar data in Section 8. Conclusions are made in Section 9.

2 Double-moment DSD normalisation

The DSD is written $N(D)$ [mm^{-1} m^{-3}], and is defined as the concentration in air of raindrops with equivolume diameter in the interval $[D, D+\delta D)$ mm. The equivolume diameter is used because raindrops become oblate with size (e.g. Thurai et al.,

2007); it is simply the diameter of a sphere that contains the same volume of water as a drop. M_n [mm^n m^{-3}], the nth-order moment of the DSD, is

$$M_n = \int_0^\infty N(D) D^n dD. \tag{1}$$

The double-moment normalisation method of Lee et al. (2004) allows for the DSD to be expressed as a combination of two of its moments M_i and M_j of arbitrary orders i and j, and a double-moment normalised DSD $h(x)$ [-], where $x = DM_i^{1/(j-i)} M_j^{-1/(j-i)}$ [-] is the second-normalised diameter (Lee et al., 2004). Using the normalisation, the DSD can be written

$$N(D) = M_i^{(j+1)/(j-i)} M_j^{(i+1)/(i-j)} h(x). \tag{2}$$

The method is flexible because the function $h(x)$ is not prescribed. Lee et al. (2004) suggested that a generalised gamma model is an appropriate choice for $h(x)$. Following their recommendation, we use the following double-moment normalised DSD (Lee et al., 2004):

$$\hat{N}(D) = M_i^{(j+1)/(j-i)} M_j^{(i+1)/(i-j)} \hat{h}(x), \tag{3}$$

$$\hat{h}(x) = c\Gamma_i^{(j+c\mu)/(i-j)} \Gamma_j^{(-i-c\mu)/(i-j)} x^{c\mu-1} \times \exp\left[-\left(\frac{\Gamma_i}{\Gamma_j}\right)^{c/(i-j)} x^c\right], \tag{4}$$

where Γ is the gamma function, $\Gamma_i = \Gamma(\mu + i/c)$ and $\Gamma_j = \Gamma(\mu + j/c)$, and c [-] and μ [-] are parameters which must be fitted to the generalised gamma model. Since this formulation allows any DSD to be described using only two of its statistical moments, the task of our DSD-retrieval algorithm is to estimate two DSD moments from polarimetric radar data.

The question of whether the double-moment normalised DSD is invariant has been investigated. Compared to previous single-moment normalisation approaches that vary by rainfall type (Sempere-Torres et al., 2000), the double-moment approach shows more similarity across such changes (Lee et al., 2004). Raupach and Berne (2017) tested the double-moment normalised DSD across spatial displacement and between different climatic regions. They showed that for practical purposes in stratiform rain and with well-chosen input moments, the double-moment DSD can be considered invariant across space with reasonable resulting performance on reconstruction of the DSD. Lee et al. (2007) showed that $h(x)$ derived from time-series measurements at one location had low scatter around the average double-moment normalised DSD. In the DSD-retrieval method proposed here, we make the assumption that the double-moment normalised DSD function $h(x)$ is invariant in space and time over the typical domain of interest, and that variance in the DSD is adequately explained through variance in two moments of the DSD.

3 Bulk rainfall variables

All bulk rainfall variables can be derived from the DSD (a detailed review is provided by Bringi and Chandrasekar, 2001). The mass-weighted mean drop diameter D_m [mm], useful as a characteristic drop size, is M_4/M_3. Liquid water content W [g m^{-3}] is related to the third moment of the DSD and is written

$$W = \frac{\pi}{6} 10^{-3} \rho_w M_3, \tag{5}$$

where ρ_w [g cm^{-3}] is the density of water. The rain rate R [mm h^{-1}] is defined as

$$R = 6\pi 10^{-4} \int_0^\infty v(D) D^3 N(D) dD, \tag{6}$$

where $v(D)$ [m s^{-1}] is the still-air terminal fall speed of a drop with equivolume diameter D. In this study $v(D)$ was calculated using the method of Beard (1976), for site-specific altitudes and latitudes, and an assumed sea-level temperature of 15° and relative humidity of 0.95.

Radar variables can also be derived from the DSD. In Rayleigh scattering, when the radar wavelength is much larger than the particles being measured and drops are assumed to be spherical, the radar reflectivity is $Z = M_6$ (Marshall et al., 1947). In Mie scattering, in which the wavelength is of similar size to the particles, reflectivity in horizontal polarisation Z_h [mm^6 m^{-3}] is defined as (Bringi and Chandrasekar, 2001)

$$Z_h = \frac{10^6 \lambda^4}{\pi^5 |K|^2} \int_0^\infty \sigma_{bh}(D) N(D) dD, \tag{7}$$

where λ [cm] is the wavelength, $|K|^2$ [-] is the dielectric factor of water, and $\sigma_{bh}(D)$ [cm^2] is the back-scattering cross-section at horizontal polarisation of a raindrop of equivolume diameter D. Reflectivity in vertical polarisation, Z_v [mm^6 m^{-3}], is obtained by replacing $\sigma_{bh}(D)$ with the vertically polarised back-scattering cross-section $\sigma_{bv}(D)$ [cm^2]. It is usual practice to deal with radar reflectivities in dBZ, calculated as $Z_H = 10 \log_{10} Z_h$ and $Z_V = 10 \log_{10} Z_v$.

Differential reflectivity Z_{DR} [dB] is $Z_H - Z_V$. Differential reflectivity in linear units, ξ_{dr} [-], defined as Z_h/Z_v, has been shown to relate to the reflectivity-weighted mean drop axis ratio r_z [-] (Jameson, 1983). r_z is defined as

$$r_z = \frac{\int_0^\infty r(D) D^6 N(D) dD}{\int_0^\infty D^6 N(D) dD}, \tag{8}$$

where $r(D)$ is the vertical to horizontal axis ratio of a drop of equivolume diameter D. The relationship found by Jameson (1983) is

$$r_z \sim (\xi_{\text{dr}})^{-\frac{3}{7}}, \tag{9}$$

which is valid for narrow distributions of raindrop axis ratio (Bringi and Chandrasekar, 2001).

Dual-polarisation radars measure specific differential phase shift (on propagation) K_{dp} [$^\circ$ km^{-1}], which is the difference in phase produced between horizontally and vertically polarised waves that pass through rain. It is defined as (Bringi and Chandrasekar, 2001)

$$K_{\text{dp}} = \frac{180\lambda}{\pi} 10^{-1} \int_0^\infty \text{Re}\left[f_{hh}(D) - f_{vv}(D)\right] N(D) dD, \tag{10}$$

where Re represents the real part of a complex number and Re(f_{hh}) [cm] and Re(f_{vv}) [cm] are the real parts of the forward scattering amplitudes for horizontal and vertical polarisation respectively. Jameson (1985) showed that K_{dp} can be linked to the product of liquid water content and the deviation from unity of the mass-weighted mean raindrop axis ratio r_m [-]. r_m is defined as

$$r_m = \frac{\int_0^\infty r(D) D^3 N(D) dD}{\int_0^\infty D^3 N(D) dD}. \tag{11}$$

K_{dp} can be written

$$K_{\text{dp}} = \left(\frac{180}{\lambda}\right) 10^{-1} CW(1 - r_m), \tag{12}$$

with dimensionless value $C \sim 3.75$ (Bringi and Chandrasekar, 2001). Various raindrop axis ratio functions are available (e.g. Pruppacher and Beard, 1970; Andsager et al., 1999; Brandes et al., 2002; Thurai et al., 2007). We return to the question of axis ratios and K_{dp} in Section 5.

The integrals in this section and Equation 1 are idealised because the range of drop sizes is written from zero to infinity. Using measured data, the integrals were calculated over truncated classes of diameter and second-normalised diameter, with D and x as class centres and dD and dx as class widths. Since truncation potentially effects bulk variables (e.g. Willis, 1984; Ulbrich, 1985; Vivekanandan et al., 2004), we used the same truncation limits for compared quantities. When polarimetric variables were calculated from DSDs, the T-matrix codes of Mishchenko and Travis (1998) were used to calculate raindrop

scattering properties, with an assumed temperature of 12.5° C, a Gaussian distribution of raindrop canting angles with zero mean and a standard deviation of 6° (stated as reasonable by Bringi and Chandrasekar, 2001), and a radar frequency of 9.4 GHz.

4 Data

To train and test the new method, data from three networks of OTT Parsivel (Löffler-Mang and Joss, 2000) disdrometers were used. Each network had a nearby X-band weather radar that scanned above the disdrometers. A full description of the data and their treatment, and the coordinates for all stations, are provided in Raupach and Berne (2017), in which the same disdrometer networks were used. Here we provide a summary of the data used in this study.

The first network provided the HyMeX data set. This network was located in Ardèche, France, in the autumns of 2012 and 2013, for the special observation periods of the Hydrological Cycle in the Mediterranean Experiment (HyMeX[1], Drobinski et al., 2014). In this study we used data from 11 first-generation Parsivel and five Parsivel^2 disdrometers located in the approximately 13×7 km^2 network. Also used were data from a METEK GmbH micro rain radar (MRR Peters et al., 2002, 2005; Tridon et al., 2011) within the network, which provided vertical profiles of estimated DSDs recorded with 100 m vertical resolution and 10 s integration time. MXPol, a transportable Doppler dual-polarisation weather radar (for instrument details see Schneebeli et al., 2013) was located to the north-east of the disdrometer network. In 2013, MXPol recorded "stacked" plan position indicator (PPI) scans above the Parsivel network at elevations of four, five, six, eight, 10, 12, 14, 16, and 20 degrees above horizontal, with a return time of about six minutes. Six rainfall events in which the MRR and MXPol both recorded data were selected for 2013. The events were from 1.8 to 7.5 hours in length. Temperature data from a weather station at Pradel Grainage were used to estimate freezing levels cutoff heights, below which precipitation was assumed to be primarily liquid. These heights ranged from 971 m to 2386 m above sea level, and only those MRR data from below the cutoff level per event were used. More network details and the list of identified events are provided in Raupach and Berne (2017). The HyMeX data set was the only set used in which estimates of the DSD aloft were available.

Two more data sets were used in order to incorporate data from different climatologies. The second instrument network was composed of five first-generation Parsivel disdrometers, and MXPol, in Payerne, Switzerland, and took measurements from February to July 2014. We used the MXPol PPI scan at five degrees above horizontal, which had a return time of about five minutes. The scans covered the region over three of the disdrometers. The third data set was from a network of 14 Parsivel^2 disdrometers (Petersen et al., 2014) deployed in Iowa, United States, during the National Aeronautics and Space Administration (NASA) Iowa Flood Studies (IFloodS) Global Precipitation Mission (GPM) ground validation campaign. Overlooking this network was the University of Iowa's X-band radar XPOL5 (Mishra et al., 2016). We used PPI data recorded at three degrees above horizontal, with a return time of about eight minutes, for three days of heavy rainfall: the 25th, 26th, and 27th May 2013. These scans covered the area over ten of the disdrometers. The three networks were in regions with different climatologies (as described in Wolfensberger et al., 2015). Table 1 provides a summary of the three networks. Table 2 shows the instruments

[1] See `http://www.hymex.org`.

covered by PPI scans, the distance of each station to the PPI radar volumes used, and the number of radar scans that overlapped with one-minute observations.

Table 1. Summary of instrument networks used. Coordinates for Parsivel networks are bounding boxes. Altitude is above sea level to nearest 10 m. Hours are provided only for non-instantaneous measurements, and show total hours of rain data across all stations.

Data set	Instrument type	Coordinates	Altitude [m]	Hours
HyMeX	Parsivel (V1 and V2)	44.5547 — 44.6141° N, 4.3826 — 4.5148° E	200 — 640	404
	MRR	44.5790° N, 4.5011° E	270	22
	X-band radar	44.6141° N, 4.5461° E	600	
Payerne	Parsivel (V1)	46.8425 — 46.9783° N, 6.9184 — 7.13° E	433 — 451	347
	X-band radar	46.8133° N, 6.9428° E	489	
Iowa	Parsivel (V2)	41.64062 — 41.99267° N, 92.09138 — 91.54163° W	197 — 286	412
	X-band radar	41.8870° N, 91.7341° W	263	

Disdrometer data, which had raw integration times of either 30 s or 60 s, and MRR data with 10 s integration time, were resampled to one-minute temporal resolution. HyMeX and Payerne Parsivel data were corrected with reference to 2D-video-disdrometer (2DVD) measurements from the HyMeX campaign (Raupach and Berne, 2015a, b). This procedure removed unrealistically large drops and those too far from expected velocities, adjusted velocity measurements, and adjusted drop concentrations so that DSD moments more closely matched those of the 2DVD. These Parsivel data were quality controlled so that only error-free time steps containing liquid precipitation were used. Iowa Parsivel data were used as provided without further quality control.

Parsivel data are subject to uncertainty due to differences across individual instruments and instrument generations (e.g. Jaffrain and Berne, 2011; Tokay et al., 2014; Thurai et al., 2011; Raupach and Berne, 2015a), and their limited sampling area introduces a bias, as reported by Tapiador et al. (2017). The Iowa data were provided in diameter class definitions that differed from those of the instrument manufacturer (Petersen et al., 2014). The HyMeX and Payerne data sets used the manufacturer's diameter class definitions, which implies the assumption of a raindrop axis ratio to equivolume diameter relationship (Battaglia et al., 2010). Our tests (not shown) showed limited differences made to DSD bulk variables when different axis ratio functions were used to modify the class definitions. Given the uncertainties involved in using modified diameter classes, we decided to use the manufacturer's class definitions for these two data sets. For each of the three regions, the Parsivel data were randomly sampled so that 60% of records formed a training data set and the remaining 40% formed an independent validation data set. Sensitivity of the random sampling was evaluated through repeated tests with different sample realisations and was found to be low.

All available disdrometer and PPI data were used, while MRR data were subset to event times so that likely solid precipitation was not considered. MRR data were attenuation-corrected (METEK, 2010; Peters et al., 2010) and contained DSDs retrieved with vertical wind ignored (Strauch, 1976; Peters et al., 2002). Negative concentrations (METEK, 2010) in MRR DSDs were

Table 2. Instrument stations with corresponding PPI volumes, with the number of scans for that volume (S), the volume centre's height above the ground (H (ground) [m], to nearest 10 m), height above sea level (H (a.s.l) [m], to nearest 10 m), and horizontal range from the radar (D [km]). MI [mm h^{-1}] is the maximum one-minute rain intensity recorded by each instrument at a radar scan time.

Network	Station	S	H (ground)	H (a.s.l)	D	MI
Payerne	HARAS Avenches	483	914	1349	9.8	15.6
	Military Airport Payerne	408	365	816	3.7	16.7
	Morat Airport	349	2087	2520	23.2	16.9
HyMeX	Lavilledieu	1209	965	1192	8.4	55.5
	Les Blaches	1256	549	978	5.4	62.3
	Lussas	1277	732	1021	6.0	67.6
	Mirabel	1254	374	870	3.8	59.3
	Mont-Redon	1267	139	775	2.5	18.7
	Pradel 1	1239	682	960	5.1	40.8
	Pradel 2	1239	682	960	5.1	36.3
	Pradel Grainage	1216	700	971	5.3	44.6
	Pradel-Grainage-v2	1216	700	971	5.3	45.1
	Pradel-Vignes	1222	733	989	5.5	22.7
	Saint-Etienne-de-Fontbellon	1099	1214	1516	13.1	53.6
	St-Germain	1139	1103	1307	10.1	76.2
	Villeneuve-de-Berg	1150	841	1142	7.7	84.0
	Villeneuve-de-Berg 2	1152	841	1142	7.7	74.2
	Villeneuve-de-Berg 3	1150	840	1141	7.7	72.5
	Pradel Grainage (MRR)	694	700 — 1850	970 — 2120	5.3	97
Iowa	apu05	94	1522	1808	29.5	49.0
	apu06	88	1566	1840	30.1	49.0
	apu07	84	1661	1933	31.9	47.6
	apu08	91	1569	1851	30.3	50.7
	apu09	110	698	938	12.9	31.4
	apu10	112	635	890	12.0	25.1
	apu11	103	600	859	11.4	25.9
	apu12	97	543	801	10.3	57.0
	apu13	102	1727	1924	31.7	65.2
	apu14	100	1727	1924	31.7	71.9

reset to zero. PPI radar reflectivities were compared to measurements from disdrometers (and the MRR in HyMeX), and bias in Z_H was corrected on a per-campaign basis. Bias in Z_{DR} was estimated using vertical scans (birdbath scans, similar to Grazioli et al., 2015), and was corrected in each of the three data sets. Two days of radar data from Payerne (2014-03-22 and 2014-04-08) exhibited higher radar bias due to hardware problems, and were not included in this study. Attenuation correction for the PPI data was performed using the ZPHI algorithm (Testud et al., 2000), and K_{dp} was estimated using the method of

Schneebeli et al. (2014). PPI scan data were sampled for instrument locations by taking the mean values of radar volumes that overlapped horizontally the instrument coordinates within the instrument's corresponding one-minute integration period. To discount noise, PPI records were subset to those for which Z_H was greater than or equal to 10 dBZ and the signal to noise ratio in horizontal polarisation was greater than or equal to 5 dB. DSD data were treated as in Raupach and Berne (2017): Parsivel DSDs were truncated to 0.2495 (0.2565) mm to 7 (7.21) mm for HyMeX and Payerne (Iowa) Parsivel data (Raupach and Berne, 2015a); to avoid including overestimated numbers of small drops (Peters et al., 2005), DSDs estimated by the MRR were truncated to 0.6 mm to 5.8 mm (Raupach and Berne, 2017) and MRR data were further subset to records with $R \leq 150$ mm h^{-1} (thus removing 0.2% of records); MRR data for altitudes greater than 2200 m were excluded because not enough points were available at those altitudes; and all DSDs were subset to time steps in which $R > 0.1$ mm h^{-1}. In each data set, more than 85% of the DSDs sampled were classified as stratiform type by Raupach and Berne (2017).

To compare measured versus estimated or retrieved values in this work, we use the median relative bias, the interquartile range (IQR) of relative bias, and the squared Pearson correlation coefficient (r^2) between reference and estimated values. If V_R is the reference value and V_E is the estimated value, the relative bias expressed as a percentage of the reference value is defined as $100(V_E - V_R)/V_R$.

5 DSD retrieval from polarimetric radar data

Raupach and Berne (2017) showed that with reasonably chosen input moments, the double-moment normalised DSD of Lee et al. (2004) can be assumed invariant across spacial displacement in stratiform rain, with a performance loss that is acceptable for practical applications. Results on limited data for non-stratiform rain types suggested that while the double-moment normalised DSD varies more in these cases, the assumption of its invariance may still lead to acceptable performance with input moments that are not both of low or both of high order. Using the assumption of an invariant double-moment normalised DSD model, the DSD can be estimated using polarimetric radar data. Given a known double-moment normalised DSD, the task of DSD reconstruction becomes that of estimating from radar information the values of two DSD moments. In this section we present a new DSD-retrieval method that uses this idea. The aim of the proposed DSD-retrieval technique is to retrieve two DSD moments using only polarimetric radar data.

The SCOP-ME method was trained with DSDs simulated using a DSD model and a wide range of DSD parameter values. In contrast, we used empirical DSDs measured by Parsivels to train our method, to avoid any assumption about the shape of the DSD. A trade-off that must be made is that the measured DSDs are truncated. However, previous studies have shown that if the considered range of drop diameters is large enough around the median drop diameter D_0 [mm], the effect of truncation on calculated bulk variables is limited (Willis, 1984; Vivekanandan et al., 2004). Willis (1984) concluded that the effect of maximum considered drop size $D_{\max}$ on bulk variables is negligible if $D_{\max}$ exceeds $2.5D_0$. Using D_0 calculated from the recorded (truncated) Parsivel DSDs, this criteria was met for 99.6% of the records. The criteria of Vivekanandan et al. (2004) is that, for there to be less than five percent error on bulk variables, the minimum drop size $D_{\min}$ should be less than $D_0/2$ and $D_{\max}$ should exceed $4D_0$. This constraint was met by 90.4% of the DSDs (93.5% met this criteria for the upper drop

size limit). Calculated D_0 may also be subject to error because of the truncation, but we consider that these calculations give broad confidence in the bulk variables we used to train the method. Further, the truncation on the Parsivel data effects primarily very small drops since large drops are rare, and therefore its influence on the higher-order moments we use is expected to be negligible.

The training data set was sampled as 60% of each of the three Parsivel data sets, and contained 182079 measured one-minute DSDs. Z_H, K_{dp} and Z_{DR} were calculated for these DSDs for the MXPol stacked PPI incidence angles, temperatures of five, 10, and 15 degrees C, and each of four drop axis ratio functions: those of Andsager et al. (1999), Brandes et al. (2002), Thurai et al. (2007), and that of Beard and Chuang (1987) in the form shown in Kalogiros et al. (2013). Unusual records with Z_{DR} or K_{dp} less than or equal to zero (0.16% of all simulated radar records) were excluded.

5.1 Retrieval of DSD moment six

Radar reflectivity in linear units, Z_h [mm^6 m^{-3}], is the sixth moment of the DSD in the Rayleigh scattering regime for spherical drops (Bringi and Chandrasekar, 2001). At X-band frequencies, larger drops enter into the Mie scattering regime and differences appear between M_6 and Z_h. We use the observation that Z_h departs from M_6 for heavier rain, and assume that this departure occurs when Z_H is greater than a threshold value. This threshold was determined through comparison of M_6 and Z_h for DSDs, classed by Z_H in classes of width 2 dBZ between 10 dBZ and 40 dBZ, and was set to 28 dBZ. For both smaller and larger reflectivity values, a power law relationship was found using orthogonal least squares fitting in log-log space. The resulting relationship is

$$\widehat{M_6} = \begin{cases} Z_h^{1.01} & \text{if } 10\log_{10}(Z_h) \leq 28 \\ 2.71\, Z_h^{0.86} & \text{if } 10\log_{10}(Z_h) > 28. \end{cases} \tag{13}$$

On the training set, median relative bias between $\widehat{M_6}$ and M_6 was 0.1%, the IQR of relative bias was 2.5 percentage points, and the r^2 value was 0.98. The fitted relationship is shown on samples of training data in Figure 1. Temperature made only limited difference to the fitted parameters: the pre-factor varied from 2.49 to 2.94 for the larger values of Z_H, and the other parameters differed by 0.01 or less from the value found for all temperatures combined.

5.2 Retrieval of DSD moment three

Retrieving a second, lower-order DSD moment is more difficult than estimating M_6, because radar variables are more closely linked to the higher-order moments of the DSD. Using theoretical relationships as much as possible, we present a method to estimate the third moment of the DSD from polarimetric data. As shown in Equation 9, the reflectivity-weighted mean drop axis ratio, r_z, is related to a negative power of the differential reflectivity in linear units. In Kalogiros et al. (2013), the reflectivity-weighted and mass-weighted drop axis ratios were assumed to be the same and differences were dealt with through fitting of qualitative relationships between radar variables. A similar approach is taken here. Since r_z and the mass-weighted

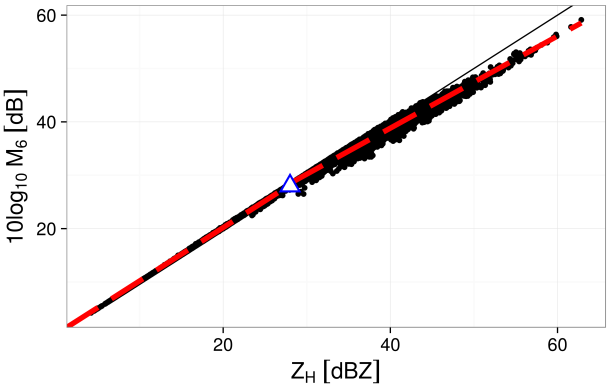

Figure 1. A sample of 20,000 points from the training set, showing the relationship between radar reflectivity and DSD moment six in dB scale. The one-to-one line is shown in black; the red dashed line shows the fitted relationship of Equation 13. The Z_H threshold of 28 dBZ is shown with a triangle.

mean drop axis ratio r_m are both weighted mean drop axis ratios, we assume that r_m is also related to differential reflectivity, and estimate r_m using a polynomial fit to Z_{DR}, such that

$$\widehat{r_m} = \sum_{i=0}^{5} c_i Z_{\text{DR}}^i. \tag{14}$$

With our training data, this polynomial of order five produced low relative bias on retrieval of M_3. Recall from Equation 5 that M_3 relates to W: substituting Equation 5 into Equation 12, and solving for M_3, we have

$$M_3 = \frac{\lambda}{0.003\pi C \rho_w} \frac{K_{\text{dp}}}{(1 - r_m)}. \tag{15}$$

At X-band (9.4 GHz, $\lambda = 3.189$ cm), assuming that $\rho_w = 1$ g cm^{-3}, and replacing r_m with its estimate based on Z_{DR}, M_3 is predicted by

$$M_3 = \frac{338.4}{\widehat{C}} \frac{K_{\text{dp}}}{(1 - \widehat{r_m})}, \tag{16}$$

where $\widehat{C}$ is a single representative value for C.

K_{dp} is sensitive to the raindrop axis ratio (e.g. Bringi and Chandrasekar, 2001), so values for c_i and $\widehat{C}$ were found per axis ratio function. The coefficients c_i in Equation 14 were found using least-squares polynomial fitting. In rare cases for large values of Z_{DR} the relationships returned unrealistic values of r_m ($0 \leq r_m$ or $r_m \geq 1$). In these few cases, $\widehat{r_m}$ was set to 0.75. Estimated $\widehat{r_m}$ values were used to find C for each training DSD, and the mean of these values was used as $\widehat{C}$. The results and

Table 3. Fitted values of $\widehat{C}$ (Equation 16) and c_i (Equation 14), by drop axis ratio function (Ratio). M_3 estimation performance in the training data is shown in terms of median relative bias (RB [%]), IQR of relative bias (IQR [% pts]), and r^2. Max Z_{DR} [dB] shows the maximum value of Z_{DR} each relationship can use.

Ratio	$\widehat{C}$	c_0	c_1	c_2	c_3	c_4	c_5	RB	IQR	r^2	Max Z_{DR}
Thurai	3.419	1	-0.075720	0.046043	-0.019965	0.003264	-0.000164	0.8	25	0.97	7.27
Brandes	3.274	1	-0.080221	0.052613	-0.023125	0.004237	-0.000279	-0.8	22	0.97	8.12
Andsager	3.220	1	-0.092664	0.074970	-0.036663	0.007466	-0.000549	-0.3	21	0.97	7.17
Beard	3.202	1	-0.088418	0.054731	-0.021392	0.003208	-0.000149	-0.7	22	0.97	7.47

their performance statistics are shown in Table 3. Fitted parameters differed across the three tested temperatures. However, parameters fitted using all training data performed similarly on training data for individual temperatures, with the median relative bias remaining within $\pm 1\%$ of the all-temperatures value, and IQR of relative bias varying by less than one percentage point. The values fitted using combined training data were used.

5.3 Summary of DSD-retrieval technique

The proposed DSD retrieval method is summarised as follows: the double-moment normalised DSD $\hat{h}(x)$ with parameters c and μ is assumed trained from data and known. Then, given K_{dp}, Z_{DR} and Z_h, (1) DSD moment six is estimated using Equation 13, and (2) DSD moment three is estimated using Equations 14 and 16 and parameters from Table 3. The DSD is then retrieved using Equation 4 with $i = 3$ and $j = 6$.

6 Comparison to an existing DSD-retrieval method

The new DSD retrieval method was compared to SCOP-ME (Anagnostou et al., 2009, 2010; Kalogiros et al., 2013). We implemented SCOP-ME using its description in Anagnostou et al. (2013). SCOP-ME was developed for X-band using simulated DSDs and T-matrix simulations of radar variables, and in Anagnostou et al. (2013) it is shown to outperform the algorithms of Anagnostou et al. (2008) and Park et al. (2005a). The DSD model used by SCOP-ME is based on the normalised DSD of Willis (1984) (see also Bringi and Chandrasekar, 2001). Kalogiros et al. (2013) provided an explicit expression for rain rate using polarimetric variables, but since we are interested in the whole DSD, in the following we compare R computed from reconstructed DSDs. The comparison of the two methods is first shown using Parsivel data in which the radar values were simulated using T-matrix codes and were therefore free of radar measurement noise.

Comparisons of the two techniques were made using the Parsivel validation data set composed of 40% of the records from HyMeX, Payerne, and Iowa. For each one-minute DSD record, Z_h, K_{dp} and Z_{DR} were calculated using T-matrix codes, for an elevation angle of 4° above horizontal, and using each of the four drop axis ratio functions. For the double-moment technique, the generalised gamma model $\hat{h}(x)$ (Equation 4) for $i = 3$ and $j = 6$ was used. $\hat{h}(x)$ was fitted to non-zero median values of $h(x)$ in classes of x with width 0.2, using weighted least squares fitting in log space, with each class weighted by its number

of observations (Raupach and Berne, 2017). The parameters found for the combined Parsivel training data were $c = 0.54$ and $\mu = 3.06$. SCOP-ME and the double-moment method were used to retrieve the DSD concentrations $N(D)$ for D in the class centres of the truncated Parsivel diameter classes. For each technique and axis ratio function, retrieved DSDs were compared to measured DSDs by comparing moments zero to seven, D_m and R.

Comparisons of relative error distributions by technique are shown in Figure 2. Example scatter plot results are shown for the HyMeX data set and the drop axis ratio model of Beard and Chuang (1987) in Figure 3. The Beard model, which has been shown to match well to observations (Thurai et al., 2009), is shown because it provided the equilibrium drop shapes around which the SCOP-ME training set was simulated (Kalogiros et al., 2013). Full performance results are shown for the HyMeX data set in Table A1, for Payerne in Table A2, and for Iowa in Table A3. The metrics used were median relative bias, IQR of relative bias, r^2, and the slope of the linear regression on measured vs. reconstructed points. Differences between the performance metrics for the two techniques were calculated such that a negative difference indicates that the double-moment technique performed better than SCOP-ME. These differences are shown visually in Figure 4, in which red colours show negative differences.

Table 4. Average differences between double-moment and SCOP-ME techniques, on Parsivel data, over three regions and four raindrop axis ratios. Negative values show an improvement by the double-moment technique over SCOP-ME.

Variable	RB	IQR	r^2	Slope
D_m	0.19	1.07	0.04	-0.07
M_0	3.67	11.97	-0.01	0.03
M_1	0.44	4.44	0.04	0.09
M_2	-0.23	0.89	0.02	-0.04
M_3	-1.28	0.46	0.00	-0.00
M_4	-0.61	2.03	-0.00	0.06
M_5	-0.49	2.36	-0.00	-0.02
M_6	-1.57	-0.22	-0.01	-0.11
M_7	-2.65	8.55	-0.03	-0.05
R	-0.98	2.06	0.00	0.07

In over half of the tested region, axis ratio function, and variable combinations, the double-moment technique produced a better median relative bias than the SCOP-ME technique, with an overall average difference of -0.35 percentage points. IQR of relative bias was usually slightly higher for the double-moment technique, with an average difference of 3.4 percentage points. Correlation coefficients and scatter plot slopes were usually similar for both techniques. The average differences across the three tested regions and four tested raindrop axis ratio functions are shown in Table 4. On average, the double-moment technique produced better median relative bias than SCOP-ME on R and DSD moments two to seven. IQRs were similar on average, with the exception of moments zero, one, and seven for which SCOP-ME produced notably smaller IQRs. As shown in Tables A1, A2, and A3, the results differed across the different drop axis ratio functions and regions. It was often the case that SCOP-ME produced a less biased estimate of DSD moment zero, but in many of these cases the double-moment technique

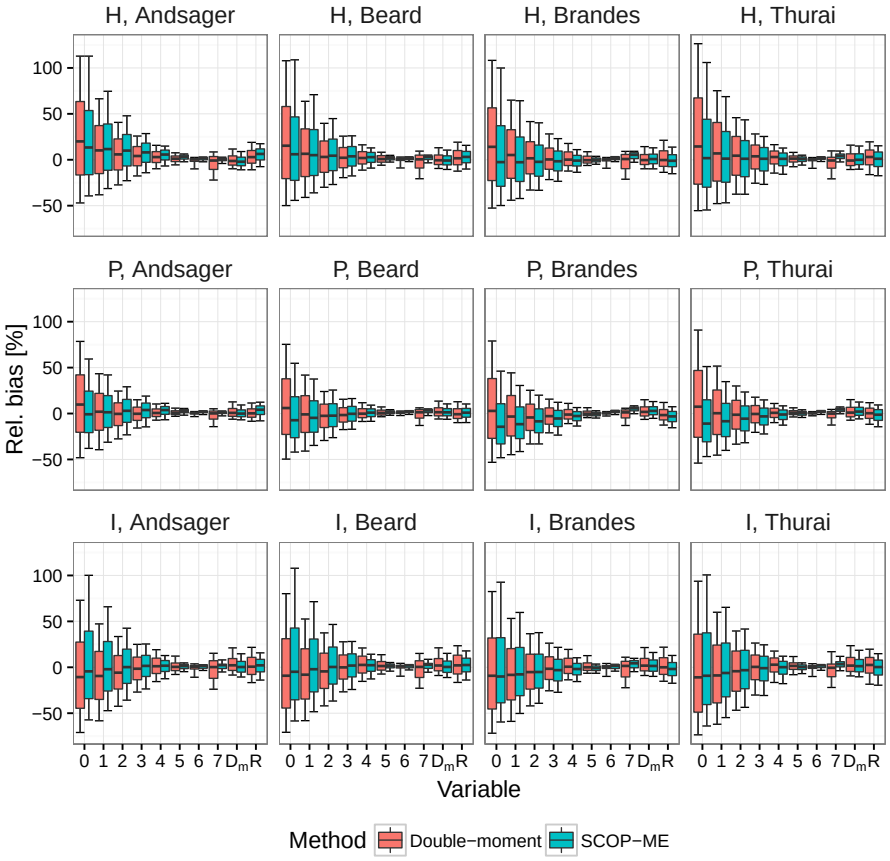

Figure 2. Relative bias distributions for the double-moment and SCOP-ME DSD-retrieval methods, by drop axis ratio function and data set (H stands for HyMeX, P for Payerne, and I for Iowa). Variables are moment order n [mm^n m^{-3}], D_m [mm], and R [mm h^{-1}]. Bold bars show medians, boxes show IQRs, whiskers show 10th to 90th percentile ranges

produced a better r^2. The double-moment technique's performance variations relate to the accuracy of the prediction of DSD moment three from K_{dp} and Z_{DR}, and to the fit of the generalised gamma function $\hat{h}(x)$. $\hat{h}(x)$ was trained on data from all data sets combined, in order to have the most general model possible. Our experiments showed that performance for low-order moments could be increased in any one region by training the gamma model on data from that region only. This aligns with the conclusions of Raupach and Berne (2017), who noted that while the double-normalised DSD can be assumed invariant for practical purposes, some residual variability remains and results in performance loss that depends on the input moments used. We now move to testing the two techniques on measured radar data, in which noise is a problem that must be dealt with.

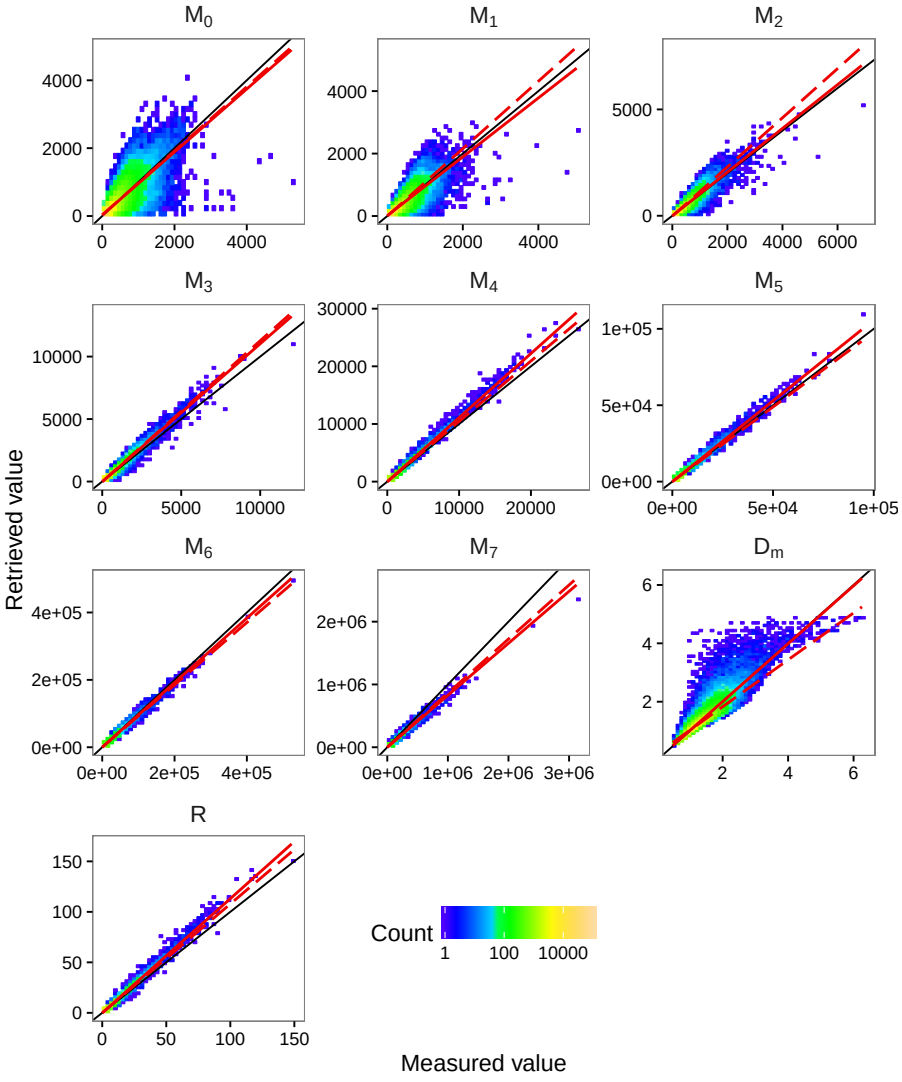

Figure 3. Density scatter plots of retrieved versus measured moments M_n [mm^n m^{-3}], R [mm h^{-1}], and D_m [mm] for the double-moment method, on the HyMeX data set, using the axis ratio function of Beard and Chuang (1987). One-to-one lines are shown in black. Regression lines for the double-moment method are shown in solid red, and dotted red lines show linear regressions for SCOP-ME, for which the densities are not shown. Values of D_m above 5 mm are extremely rare; less than 0.02% of DSDs in each data set show these values.

7 Reducing the effects of noise

Radar data is noisy at light rain rates, particularly for K_{dp} and Z_{DR} (e.g. Bringi et al., 2002; Schneebeli et al., 2014). We propose here a method to deal with this noise for the current application of DSD retrieval. Regressions on Z_h and ξ_{dr} are used

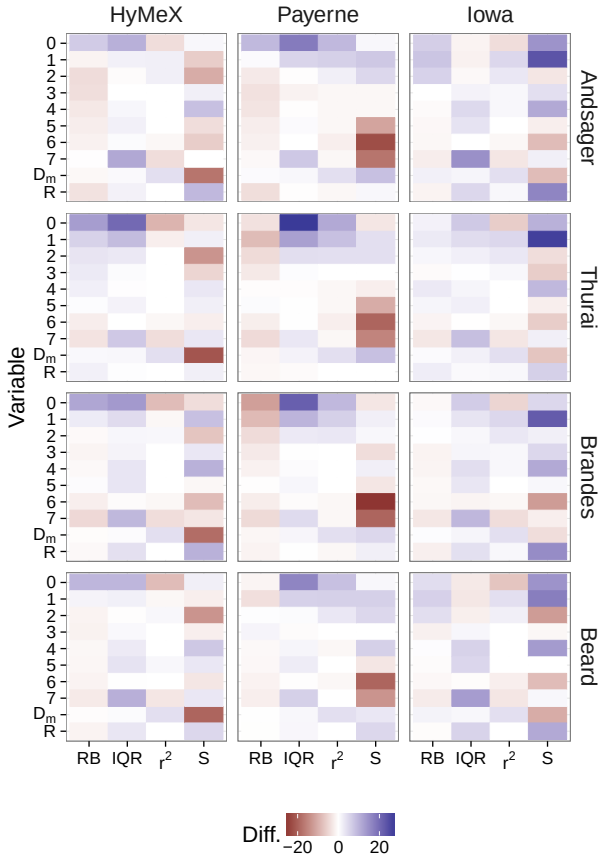

Figure 4. Differences in performance between the double-moment technique and SCOP-ME, using radar variables simulated from Parsivel data, by region and drop axis ratio function (differences in Tables A1, A2, and A3). Reds indicate negative differences, where the double-moment technique outperformed SCOP-ME. Variables are moment order n [mm^n m^{-3}], D_m [mm], and R [mm h^{-1}]. Differences are shown for median relative bias (RB [% pts]), IQR of relative bias (IQR [% pts]), r^2 (difference in deviations from unity, multiplied by 100 for display on this scale), and regression slope (S, difference in deviations from unity, multiplied by 100).

to determine "expected" values for these variables, which can be used when the measured values are likely to be noisy. We found that Z_{DR} can be reasonably predicted from Z_h using

$$\hat{Z}_{\mathrm{DR}} \sim \alpha_Z Z_h^{\beta_Z}, \tag{17}$$

and K_{dp} can be predicted from Z_h and ξ_{dr} using

$$\hat{K}_{\mathrm{dp}} \sim \alpha_K Z_h^{\beta_{K1}} \xi_{\mathrm{dr}}^{\beta_{K2}} \tag{18}$$

Table 5. Fitted coefficients and the performance of the fits on the training data, for Equations 17 and 18, by raindrop axis ratio function (Ratio). Performance is shown in terms of median relative bias (RB [%]) and the IQR [% pts] of relative bias.

			Z_{DR} performance					K_{dp} performance	
Ratio	α_Z	β_Z	RB	IQR	α_K	β_{K1}	β_{K2}	RB	IQR
Thurai	0.030	0.436	-5	64	0.00010	1.057	-3.171	-1	19
Brandes	0.027	0.449	-4	70	0.00010	1.037	-2.723	-1	13
Andsager	0.043	0.377	-3	57	0.00017	0.976	-3.262	0	16
Beard	0.048	0.384	-4	59	0.00017	1.015	-3.365	-0	13

with parameters α_Z, β_Z, α_K, β_{K1} and β_{K2}. Least-squares fitting in log-log space, using the training data set described in Section 5, was used to find best-fitting parameter values per raindrop axis ratio function. Just as for the retrieval of DSD moment six, assumed air temperature made only a small difference (parameter values fitted to individual temperature data sets differed by less than 4% from those fitted using combined temperatures), whereas different axis ratios produced more diverse parameter values. Resulting parameter values and performance statistics are shown in Table 5.

Threshold values are used to determine when K_{dp} and Z_{DR} may be noisy. A threshold value on Z_H selects values of Z_H for which K_{dp} and Z_{DR} showed large variation around their expected values in the three radar data sets used here. Threshold values on Z_{DR} and K_{dp} are those of Bringi et al. (2002). To reduce the effects of noise, then, if $Z_H < 37$ dBZ or $Z_{DR} < 0.2$ dB, measured Z_{DR} is replaced by the the expected value $\hat{Z}_{DR}$ and ξ_{dr} is replaced by $10^{(\hat{Z}_{DR}/10)}$. Likewise, if $Z_H < 37$ dBZ or $K_{dp} < 0.3\ ^\circ\ km^{-1}$, K_{dp} is replaced by $\hat{K}_{dp}$ (calculated with $\hat{\xi_{dr}}$ if ξ_{dr} was replaced). This treatment method allows radar data with negative or zero K_{dp} or Z_{DR} to be used. The treatment improved DSD-retrieval performance for both the double-moment and SCOP-ME techniques. For example, when retrieved DSDs were matched to measured MRR data (Section 8.1), the median relative bias was reduced by an average (across variables) of ~6 percentage points for SCOP-ME and by ~16 percentage points for the double-moment technique, while average IQRs were reduced more; for example on the comparison with MRR data the IQRs were reduced by ~81 (69) percentage points for the SCOP-ME (double-moment) method. When retrieved DSDs were compared to Parsivel data (Section 8.2), the noise in the radar data contributed to errors to such an extent that for both techniques the proposed treatment reduced the IQR and at times the median of relative bias by hundreds of percentage points for some variables. We note that because most values of Z_H recorded in the PPIs analysed here were lower than 37 dBZ, the noise correction affected the majority of radar records.

8 Comparisons using radar data

The DSD-retrieval techniques were applied to PPI radar data from the three locations. The double-moment technique was run on noise-corrected data. SCOP-ME was run on uncorrected PPI data (subset to $K_{dp} > 0$ and $Z_{DR} > 0$) and noise-corrected data. We used the elevation angles of the stacked PPIs for HyMeX, 5° for Payerne, and 3° for Iowa. Measured radar variables Z_H, K_{dp} and Z_{DR} were recovered for volumes corresponding to instrument locations. DSD retrieval was performed using these

values, and the resulting DSDs compared to those that were measured by other instruments. All comparisons using PPI data involved a difference in measurement volume – a change-of-support problem that we expect will introduce error spread (e.g. Raupach and Berne, 2016). There were, at times, significant vertical distances between the radar volume and the ground-based Parsivels used in these comparisons (see Table 2). These factors and uncertainty in the noise correction technique combine to create greater uncertainty in the comparisons of the two techniques made using real data than in those made using simulated radar variables from disdrometer data.

Because the axis ratio of Thurai et al. (2007) produced good results using the double-moment technique on the Parsivel data, the double-moment technique was used with parameters for this axis ratio function. Note that the assumption of axis ratio function affects only parameters of the double-moment technique, because the radar data used in this section are measured, not simulated, and the SCOP-ME technique is used as presented in Anagnostou et al. (2013). In the HyMeX campaign, the lowest available PPI elevation angle (4°) was used to compare results to Parsivels, but there was also an MRR at Pradel Grainage which retrieved estimates of the DSD aloft. MRR-derived DSDs were compared at eight different altitudes using the MXPol stacked PPIs (except 20° elevation) above the HyMeX instrument network. We first address the comparisons with MRR for HyMeX, then move to the comparisons with the Parsivel networks in all three regions.

8.1 Comparisons to MRR DSD estimates aloft

MXPol volume centre altitudes were projected onto MRR altitude classes for comparison. The double-moment DSD-retrieval algorithm was used with generalised gamma model $\hat{h}$ parameters (Equation 4) for MRR data and $i = 3$ and $j = 6$. These parameters were found using the same fitting technique as for Parsivel data (Section 6), but differ since instrumental differences produce different forms of $h(x)$ (Raupach and Berne, 2017). The parameters were set to $c = 0.4$ and $\mu = 32.25$ (the value of μ was reduced from 32.28 to stay within the computational limits of the software used). The large value of μ is due to the large numbers of small drops returned by the DSD-retrieval algorithm used by the MRR (Raupach and Berne, 2017), and is compensated somewhat by the small value of c. The reconstructed DSDs were found for classes of drop diameter from 0.65 to 5.75 mm with a class width of 0.1 mm, so that the reconstructed truncation matched that of the MRR data. PPI values from eight 100 m altitude classes between about 900 and 2100 m above sea level were compared to MRR estimates of the DSD aloft. Two output pairings are shown here: the first in which both techniques used noise-corrected data, and the second in which the SCOP-ME technique used raw data and the double-moment technique used the same raw data set corrected for noise. This second pairing was made to ensure that the performance of SCOP-ME was not compromised by the noise-correction technique.

Results of comparisons between MRR- and PPI-derived DSDs are shown for three example altitudes in Figure 5. There was good agreement between the recorded radar reflectivity recorded by both instruments, with a median relative bias of -3%, an IQR on relative bias of 16 percentage points, and a value of r^2 of 0.63. The improvement in SCOP-ME performance made by the noise correction is clear. When both techniques used noise-corrected input, both overestimated DSD moment orders zero to four and underestimated orders six and seven. Rain rate was recovered with a median relative bias of 2% (IQR 94 % pts) by the double-moment technique and 17% (IQR 106 % pts) by SCOP-ME. The double-moment technique showed lower median relative bias than SCOP-ME on moments one to four, seven, and R, and smaller IQRs on moment two to six, D_m, and

R. Similar to some of the Parsivel results, the double-moment technique overestimated moments zero and one of the DSD. r^2 values were low for both techniques (the maximum was 0.31, by SCOP-ME for D_m), but the double-moment technique had the same or a slightly higher value of r^2 in the majority of cases. High best-fit slopes were observed for both techniques for moments five, six, and seven, and show the effect of a few outlier points in these cases. Performance differences between the two techniques using noise-corrected data are shown in Table A4. Overall, the double-moment technique for DSD-retrieval out-performed SCOP-ME for the retrieval of DSD moments above order zero and rain rate measured aloft by the MRR.

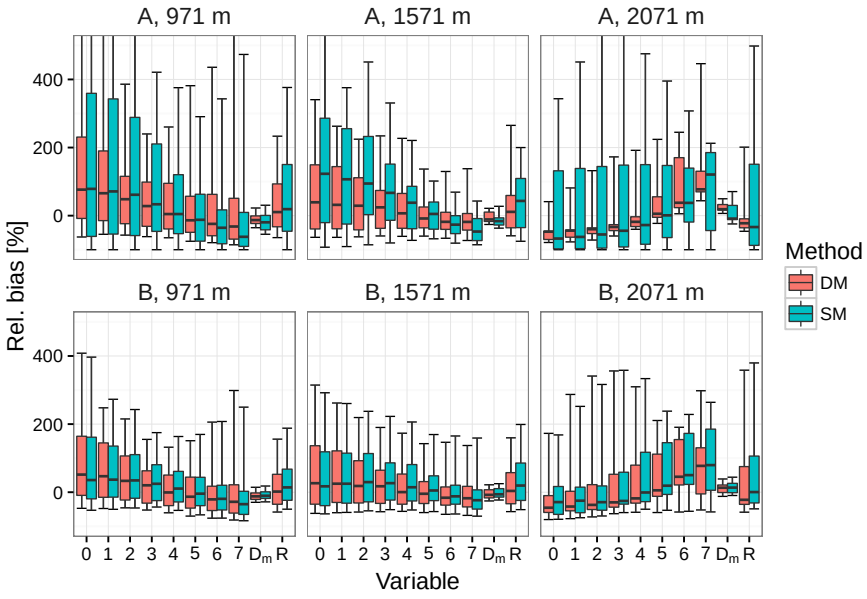

Figure 5. Distributions of relative bias on DSD moments zero to seven, comparing DSDs retrieved using PPI data to those measured by the MRR at Pradel Grainage. The results are classed by altitude for a selection of three altitudes across the compared range. Two comparisons are shown: in comparison A, SCOP-ME used raw PPI data and the double-moment technique used the noise-corrected version of the same data set. In B, both techniques used noise-corrected data sets. Symbols as for Figure 2.

8.2 Comparisons to DSDs measured by Parsivels

DSDs retrieved from polarimetric radar data were also compared to those recorded by ground-based Parsivels in the three regions we studied. Unlike in previous sections where training and validation divisions of the Parsivel data were used, here we compared DSDs derived using independent radar data to all available matching Parsivel records. The DSDs were retrieved in truncated Parsivel drop diameter classes, using the Parsivel generalised gamma model parameters quoted in Section 6. In the Payerne and Iowa data sets, the noise-correction routine was required in order to retrieve realistic DSDs; the results shown here are thus for the SCOP-ME and double-moment techniques both run on noise-corrected PPI data. Figure 6 shows distributions of DSD-retrieval relative error for each region.

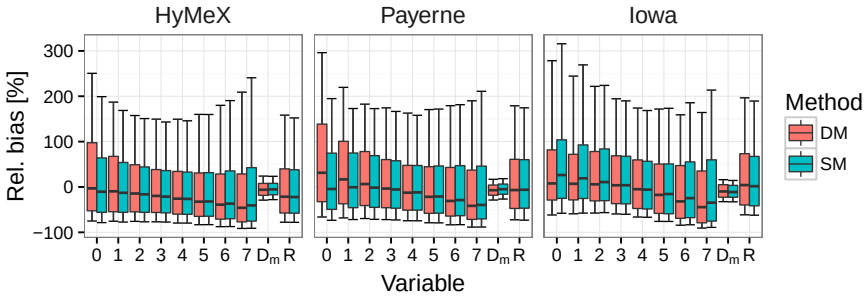

Figure 6. Distributions of relative bias on DSD moments zero to seven, comparing DSDs retrieved using noise-corrected PPI data, and those measured by Parsivel networks. Symbols as for Figure 2.

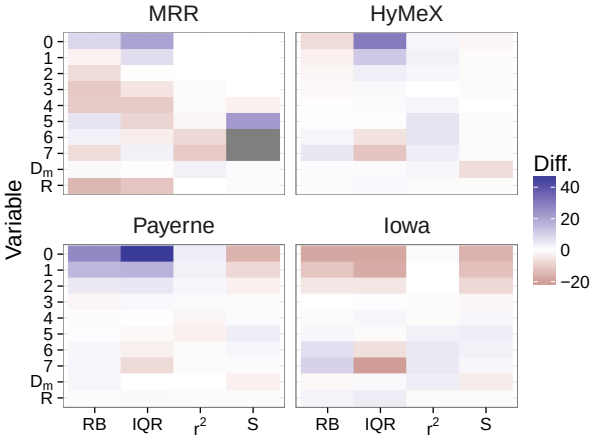

Figure 7. Differences in performance between the double-moment technique and SCOP-ME using noise-corrected radar data, for MRR and for Parsivels by region (differences in Table A4). Variables and performance statistics as for Figure 4. Red indicates that the double-moment technique outperformed SCOP-ME. Grey indicates an r^2 difference greater than 50 on this scale; these slopes were affected by outliers.

The double-moment technique produced smaller ranges of relative bias than SCOP-ME for moments five, six, and seven. For moment orders zero and one, the double-moment technique produced better median relative bias than SCOP-ME in the HyMeX and Iowa data sets, but worse in Payerne. Where the double-moment technique produced better median relative bias, the average improvement was of four percentage points, while in cases where SCOP-ME performed better, the average improvement was five percentage points. Values of r^2 and scatter plot slope were similar between the two techniques, with the majority of cases showing differences of less than 0.05 for both variables. Differences in performance between the two techniques are shown in Figure 7 and Table A4.

The performance of the double-moment technique is reliant on how accurately two DSD moments can be extracted from radar data, and in turn on how accurate the radar data are. Both retrieval techniques appear to be similarly affected by radar inaccuracies such as bias in Z_H, and experiments with different reflectivity bias corrections (not shown here) showed similar patterns of results. In Parsivel comparisons, the proposed DSD-retrieval technique was applied using a single double-moment normalised DSD model in all three tested regions, without significant performance loss between regions. This supports previous findings (Raupach and Berne, 2017) that for practical use with real radar data in primarily stratiform rain, the double-moment normalised DSD may be considered invariant in regions at similar latitudes.

9 Conclusions

Given the assumption of an invariant normalised DSD, and an estimate of that function, the DSD can be predicted using only two of its moments using the double-moment normalisation method of Lee et al. (2004). Two DSD moments are available from polarimetric radar data. At X-band, radar reflectivity can be used to accurately predict the sixth moment of the DSD, and moment three can be retrieved relatively accurately using K_{dp} and Z_{DR}. We showed that by estimating these two DSD moments from radar data, the DSD for a radar volume can be predicted using the double-moment formulation. Tests on disdrometer data from three networks in different climatic regions showed that DSD-retrieval using this new technique produced similar or slightly better performance than the SCOP-ME DSD-retrieval technique of Kalogiros et al. (2013). The proposed method is also more flexible, because there is no prescribed functional form for the double-moment normalised DSD, and even a non-parametric $\hat{h}(x)$ could be used. Nor is there a prescribed method of DSD moment extraction, which means that the moments used could be tailored to the intended purpose.

A new method for treatment of radar data with possibly noisy values of K_{dp} and Z_{DR} was proposed. The method is based on predicting the expected values of these variables from radar reflectivity, and considerably improved the performance of both the DSD-retrieval techniques. DSDs were predicted from polarimetric variables in noise-corrected PPI scans measured by X-band radars in each of the three regions. Comparisons of the retrieved DSDs to MRR data for DSDs aloft in the HyMeX region in France, and of radar-retrieved DSDs to disdrometer data from the three regions, showed reasonable agreement but large error spread for both methods. This study provides a proof-of-concept for DSD-retrieval using noise-corrected radar data, the double-moment normalisation method of (Lee et al., 2004), and a generalised gamma model for the normalised DSD. Performance improvements may be possible through future work, that should test the approach using different instruments and data sets, address more precise prediction of low-order DSD moments from polarimetric radar data, and investigate different models and fitting methods for the double-moment normalised DSD..

Acknowledgements. For deploying and maintaining the instruments used, we thank, for HyMeX: J. Jaffrain, M. Schleiss, J. Grazioli, D. Wolfensberger, A. Studzinski (EPFL LTE), B. Boudevillain, G. Molinié, S. Gérard (Laboratoire d'étude des Transferts en Hydrologie et Environnement (LTHE), Grenoble University), Y. Pointin and J. Van Baelen (Laboratoire de Météorologie Physique (LaMP), Université Blaise Pascal de Clermont-Ferrand). For Payerne: J. Jaffrain and Meteosuisse. We thank J. Grazioli for processing the MRR and radar data sets.

HyMeX data were obtained from the HyMeX program, sponsored by grants MISTRALS/HyMeX, ANR-2011-BS56-027 FLOODSCALE project, OHMCV & EPFL-LTE. We thank the Swiss National Science Foundation for financial support under grant 2000021_140669. We thank two anonymous reviewers for their constructive reviews.

References

Anagnostou, M. N., Anagnostou, E. N., Vulpiani, G., Montopoli, M., Marzano, F. S., and Vivekanandan, J.: Evaluation of X-Band Polarimetric-Radar Estimates of Drop-Size Distributions From Coincident S-Band Polarimetric Estimates and Measured Raindrop Spectra, IEEE T. Geosci. Remote Sens., 46, 3067–3075, doi:10.1109/TGRS.2008.2000757, 2008.

Anagnostou, M. N., Kalogiros, J., Anagnostou, E. N., and Papadopoulos, A.: Experimental results on rainfall estimation in complex terrain with a mobile X-band polarimetric weather radar, Atmos. Res., 94, 579–595, doi:10.1016/j.atmosres.2009.07.009, 2009.

Anagnostou, M. N., Kalogiros, J., Anagnostou, E. N., Tarolli, M., Papadopoulos, A., and Borga, M.: Performance evaluation of high-resolution rainfall estimation by X-band dual-polarization radar for flash flood applications in mountainous basins, J. Hydrol., 394, 4–16, doi:10.1016/j.jhydrol.2010.06.026, 2010.

Anagnostou, M. N., Kalogiros, J., Marzano, F. S., Anagnostou, E. N., Montopoli, M., and Piccioti, E.: Performance Evaluation of a New Dual-Polarization Microphysical Algorithm Based on Long-Term X-Band Radar and Disdrometer Observations, J. Hydrometeor., 14, 560–576, doi:10.1175/JHM-D-12-057.1, 2013.

Andsager, K., Beard, K. V., and Laird, N. F.: Laboratory measurements of axis ratios for large rain drops, J. Atmos. Sci., 56, 2673–2683, doi:10.1175/1520-0469(1999)056<2673:LMOARF>2.0.CO;2, 1999.

Atlas, D. and Ulbrich, C.: Drop size spectra and integral remote sensing parameters in the transition from convective to stratiform rain, Geophys. Res. Lett., 33, doi:10.1029/2006GL026824, 2006.

Baldauf, M., Seifert, A., Förstner, J., Majewski, D., Raschendorfer, M., and Reinhardt, T.: Operational convective-scale numerical weather prediction with the COSMO model: description and sensitivities, Mon. Weather Rev., 139, 3887–3905, doi:10.1175/MWR-D-10-05013.1, 2011.

Battaglia, A., Rustemeier, E., Tokay, A., Blahak, U., , and Simmer, C.: PARSIVEL snow observations: a critical assessment, J. Atmos. Oceanic Technol., 27, 333–344, doi:10.1175/2009JTECHA1332.1, 2010.

Beard, K. V.: Terminal velocity and shape of cloud and precipitation drops aloft, J. Atmos. Sci., 33, 851–864, doi:10.1175/1520-0469(1976)033<0851:TVASOC>2.0.CO;2, 1976.

Beard, K. V. and Chuang, C.: A new model for the equilibrium shape of raindrops, J. Atmos. Sci., 44, 1509–1524, doi:10.1175/1520-0469(1987)044<1509:ANMFTE>2.0.CO;2, 1987.

Brandes, E., Zhang, G., and Vivekanandan, J.: Experiments in rainfall estimation with a polarimetric radar in a subtropical environment, J. Appl. Meteor., 41, 674–685, 2002.

Brandes, E. A., Zhang, G., and Vivekanandan, J.: An Evaluation of a Drop Distribution-Based Polarimetric Radar Rainfall Estimator, Journal of Applied Meteorology, 42, 652–660, doi:10.1175/1520-0450(2003)042<0652:AEOADD>2.0.CO;2, 2003.

Brandes, E. A., Zhang, G., and Vivekanandan, J.: Drop size distribution retrieval with polarimetric radar: Model and application, J. Appl. Meteor., 43, 461–475, doi:10.1175/1520-0450(2004)043<0461:DSDRWP>2.0.CO;2, 2004a.

Brandes, E. A., Zhang, G., and Vivekanandan, J.: Comparison of Polarimetric Radar Drop Size Distribution Retrieval Algorithms, Journal of Atmospheric and Oceanic Technology, 21, 584–598, doi:10.1175/1520-0426(2004)021<0584:COPRDS>2.0.CO;2, 2004b.

Bringi, V., Huang, G.-J., Chandrasekar, V., and Gorgucci, E.: A methodology for estimating the parameters of a gamma raindrop size distribution model from polarimetric radar data: Application to a squall-line event from the TRMM/Brazil campaign, J. Atmos. Oceanic Technol., 19, 633–645, doi:10.1175/1520-0426(2002)019<0633:AMFETP>2.0.CO;2, 2002.

Bringi, V., Tolstoy, L., Thurai, M., and Petersen, W.: Estimation of Spatial Correlation of Drop Size Distribution Parameters and Rain Rate Using NASA's S-Band Polarimetric Radar and 2D Video Disdrometer Network: Two Case Studies from MC3E, Journal of Hydrometeorology, 16, 1207–1221, doi:10.1175/JHM-D-14-0204.1, 2015.

Bringi, V. N. and Chandrasekar, V.: Polarimetric Doppler weather radar, Cambridge University Press, 2001.

Bringi, V. N., Chandrasekar, V., Hubbert, J., Gorgucci, E., Randeu, W. L., and Schoenhuber, M.: Raindrop Size Distribution in Different Climatic Regimes from Disdrometer and Dual-Polarized Radar Analysis, J. Atmos. Sci., 60, 354–365, doi:10.1175/1520-0469(2003)060<0354:RSDIDC>2.0.CO;2, 2003.

Cao, Q. and Zhang, G.: Errors in Estimating Raindrop Size Distribution Parameters Employing Disdrometer and Simulated Raindrop Spectra, J. Appl. Meteor. Climate, 48, 406–425, doi:10.1175/2008JAMC2026.1, 2009.

Drobinski, P., Ducrocq, V., Alpert, P., Anagnostou, E., Béranger, K., Borga, M., Braud, I., Chanzy, A., Davolio, S., Delrieu, G., Estournel, C., Filali Boubrahmi, N., Font, J., Grubisic, V., Gualdi, S., Homar, V., Ivancan-Picek, B., Kottmeier, C., Kotroni, V., Lagouvardos, K., Lionello, P., Llasat, M. C., Ludwig, W., Lutoff, C., Mariotti, A., Richard, E., Romero, R., Rotunno, R., Roussot, O., Ruin, I., Somot, S., Taupier-Letage, I., Tintore, J., Uijlenhoet, R., and Wernli, H.: HyMeX, a 10-year multidisciplinary program on the Mediterranean water cycle, Bull. Amer. Meteor. Soc., 95, doi:10.1175/BAMS-D-12-00242.1, 2014.

Gorgucci, E., Chandrasekar, V., Bringi, V. N., and Scarchilli, G.: Estimation of Raindrop Size Distribution Parameters from Polarimetric Radar Measurements, J. Atmos. Sci., 59, 2373–2384, doi:10.1175/1520-0469(2002)059<2373:EORSDP>2.0.CO;2, 2002.

Gorgucci, E., Chandrasekar, V., and Baldini, L.: Microphysical Retrievals from Dual-Polarization Radar Measurements at X Band, J. Atmos. Oceanic Technol., 25, 729–741, doi:10.1175/2007JTECHA971.1, 2008.

Grazioli, J., Tuia, D., and Berne, A.: Hydrometeor classification from polarimetric radar measurements: a clustering approach, Atmos. Meas. Tech., 8, 149–170, doi:10.5194/amt-8-149-2015, 2015.

Illingworth, A. J. and Blackman, T. M.: The need to represent raindrop size spectra as normalized gamma distributions for the interpretation of polarization radar observations, J. Appl. Meteor., 41, 286–297, doi:10.1175/1520-0450(2002)041<0286:TNTRRS>2.0.CO;2, 2002.

Jaffrain, J. and Berne, A.: Experimental quantification of the sampling uncertainty associated with measurements from Parsivel disdrometers, J. Hydrometeor., 12, doi:10.1175/2010JHM1244.1, 2011.

Jaffrain, J. and Berne, A.: Quantification of the small-scale spatial structure of the raindrop size distribution from a network of disdrometers, J. Appl. Meteor. Climate, 51, doi:10.1175/JAMC-D-11-0136.1, 2012.

Jameson, A. R.: Microphysical Interpretation of Multi-Parameter Radar Measurements in Rain. Part I: Interpretation of Polarization Measurements and Estimation of Raindrop Shapes, Journal of the Atmospheric Sciences, 40, 1792–1802, doi:10.1175/1520-0469(1983)040<1792:MIOMPR>2.0.CO;2, 1983.

Jameson, A. R.: Microphysical interpretation of multiparameter radar measurements in rain. Part III: Interpretation and measurement of propagation differential phase shift between orthogonal linear polarizations, J. Atmos. Sci., 42, 607–614, doi:10.1175/1520-0469(1985)042<0607:MIOMRM>2.0.CO;2, 1985.

Jameson, A. R. and Kostinski, A. B.: What is a raindrop size distribution?, Bull. Amer. Meteor. Soc., 82, 1169–1177, doi:10.1175/1520-0477(2001)082<1169:WIARSD>2.3.CO;2, 2001.

Kalogiros, J., Anagnostou, M. N., Anagnostou, E. N., Montopoli, M., Picciotti, E., and Marzano, F. S.: Optimum Estimation of Rain Microphysical Parameters From X-Band Dual-Polarization Radar Observables, IEEE T. Geosci. Remote Sens., 51, 3063–3076, doi:10.1109/TGRS.2012.2211606, 2013.

Lee, G., Zawadzki, I., Szyrmer, W., Sempere-Torres, D., and Uijlenhoet, R.: A general approach to double-moment normalization of drop size distributions, J. Appl. Meteor., 43, 264–281, doi:10.1175/1520-0450(2004)043<0264:AGATDN>2.0.CO;2, 2004.

Lee, G. W., Seed, A. W., and Zawadzki, I.: Modeling the variability of drop size distributions in space and time, Journal of applied meteorology and climatology, 46, 742–756, doi:10.1175/JAM2505.1, 2007.

Löffler-Mang, M. and Joss, J.: An optical disdrometer for measuring size and velocity of hydrometeors, J. Atmos. Oceanic Technol., 17, 130–139, doi:10.1175/1520-0426(2000)017<0130:AODFMS>2.0.CO;2, 2000.

Marshall, J. S., Langille, R. C., and Palmer, W. M.: Measurement of rainfall by radar, J. Meteor., 4, 186–192, doi:10.1175/1520-0469(1947)004<0186:MORBR>2.0.CO;2, 1947.

Matrosov, S. Y., Kingsmill, D. E., Martner, B. E., and Ralph, F. M.: The Utility of X-Band Polarimetric Radar for Quantitative Estimates of Rainfall Parameters, Journal of Hydrometeorology, 6, 248–262, doi:10.1175/JHM424.1, 2005.

METEK: MRR Physical Basics, Tech. rep., METEK Metorologische Messtechnik GmbH, Elmshom, Germany, updated 2012-03-13, valid for MRR Service Version $\geq$ 5.2.0.9, 2010.

Mishchenko, M. I. and Travis, L. D.: Capabilities and limitations of a current FORTRAN implementation of the T-matrix method for randomly oriented, rotationally symmetric scatterers, J. Quant. Spectrosc. Radiat. Transfer, 60, 309–324, doi:10.1016/S0022-4073(98)00008-9, 1998.

Mishra, K. V., Krajewski, W. F., Goska, R., Ceynar, D., Seo, B.-C., Kruger, A., Niemeier, J. J., Galvez, M. B., Thurai, M., Bringi, V. N., Tolstoy, L., Kucera, P. A., Petersen, W. A., Grazioli, J., and Pazmany, A. L.: Deployment and Performance Analyses of High-Resolution Iowa XPOL Radar System during the NASA IFloodS Campaign, J. Hydrometeor., 17, 455–479, doi:10.1175/JHM-D-15-0029.1, 2016.

Moisseev, D. N. and Chandrasekar, V.: Examination of the μ-Λ relation suggested for drop size distribution parameters, J. Atmos. Oceanic Technol., 24, 847–855, doi:10.1175/JTECH2010.1, 2007.

Park, S.-G., Bringi, V. N., Chandrasekar, V., Maki, M., and Iwanami, K.: Correction of Radar Reflectivity and Differential Reflectivity for Rain Attenuation at X Band. Part I: Theoretical and Empirical Basis, J. Atmos. Oceanic Technol., 22, 1621–1632, doi:10.1175/JTECH1803.1, 2005a.

Park, S.-G., Maki, M., Iwanami, K., Bringi, V. N., and Chandrasekar, V.: Correction of Radar Reflectivity and Differential Reflectivity for Rain Attenuation at X Band. Part II: Evaluation and Application, J. Atmos. Oceanic Technol., 22, 1633–1655, doi:10.1175/JTECH1804.1, 2005b.

Peters, G., Fischer, B., and Andersson, T.: Rain observations with a vertically looking Micro Rain Radar (MRR), Boreal Environ. Res., 7, 353–362, 2002.

Peters, G., Fischer, B., Münster, H., Clemens, M., and Wagner, A.: Profiles of raindrop size distributions as retrieved by microrain radars, J. Appl. Meteor., 44, 1930–1949, doi:10.1175/JAM2316.1, 2005.

Peters, G., Fischer, B., and Clemens, M.: Rain Attenuation of Radar Echoes Considering Finite-Range Resolution and Using Drop Size Distributions, Journal of Atmospheric and Oceanic Technology, 27, 829–842, doi:10.1175/2009JTECHA1342.1, 2010.

Petersen, W. A., Tokay, A., Gatlin, P. N., and Wingo, M. T.: GPM Ground Validation Autonomous Parsivel Unit (APU) IFloodS [APU quality controlled drop size distributions], doi:10.5067/GPMGV/IFLOODS/APU/DATA301, https://fcportal.nsstc.nasa.gov/pub/gpm_validation/ifloods/disdrometers_and_gauges/parsivel/, dataset available online from the NASA Global Hydrology Resource Center DAAC, Huntsville, Alabama, U.S.A., 2014.

Pruppacher, H. and Beard, K.: A wind tunnel investigation of the internal circulation and shape of water drops falling at terminal velocity in air, Q. J. Roy. Meteor. Soc., 96, 247–256, doi:10.1002/qj.49709640807, 1970.

Pruppacher, H. R. and Klett, J. D.: Microphysics of clouds and precipitation, Kluwer Academic Publishers, Dordrecht, 2nd rev. and enl. ed., with an introduction to cloud chemistry and cloud electricity edn., 2000.

Raupach, T. H. and Berne, A.: Correction of raindrop size distributions measured by Parsivel disdrometers, using a two-dimensional video disdrometer as a reference, Atmos. Meas. Tech., 8, 343–365, doi:10.5194/amt-8-343-2015, http://www.atmos-meas-tech.net/8/343/2015/, 2015a.

Raupach, T. H. and Berne, A.: Corrigendum to "Correction of raindrop size distributions measured by Parsivel disdrometers, using a two-dimensional video disdrometer as a reference" published in Atmos. Meas. Tech., 8, 343-365, 2015, Atmos. Meas. Tech., doi:10.5194/amt-8-343-2015-corrigendum, http://www.atmos-meas-tech.net/8/343/2015/, 2015b.

Raupach, T. H. and Berne, A.: Small-scale variability of the raindrop size distribution and its effect on areal rainfall retrieval, J. Hydrometeor., 17, 2077–2104, doi:10.1175/JHM-D-15-0214.1, 2016.

Raupach, T. H. and Berne, A.: Invariance of the double-moment normalized raindrop size distribution through 3D spatial displacement in stratiform rain, J. Appl. Meteor. Climate, in press, 2017.

Schneebeli, M., Dawes, N., Lehning, M., and Berne, A.: High-resolution vertical profiles of polarimetric X-band weather radar observables during snowfall in the Swiss Alps, J. Appl. Meteor. Climate, 52, 378–394, doi:10.1175/JAMC-D-12-015.1, 2013.

Schneebeli, M., Grazioli, J., and Berne, A.: Improved estimation of the specific differential phase shift using a compilation of Kalman filter ensembles, IEEE T. Geosci. Remote Sens., 52, 5137–5149, doi:10.1109/TGRS.2013.2287017, 2014.

Seliga, T. and Bringi, V.: Potential use of radar differential reflectivity measurements at orthogonal polarizations for measuring precipitation, J. Appl. Meteor., 15, 69–76, doi:10.1175/1520-0450(1976)015<0069:PUORDR>2.0.CO;2, 1976.

Sempere-Torres, D., Sanchez-Diezma, R., Zawadzki, I., and Creutin, J.: Identification of stratiform and convective areas using radar data with application to the improvement of DSD analysis and ZR relations, Physics and Chemistry of the Earth, Part B: Hydrology, Oceans and Atmosphere, 25, 985–990, doi:10.1016/S1464-1909(00)00138-6, 2000.

Strauch, R. G.: Theory and application of the FW-CW doppler radar, Ph.D. Thesis Colorado Univ., Boulder., 1976.

Tapiador, F., Checa, R., and De Castro, M.: An experiment to measure the spatial variability of rain drop size distribution using sixteen laser disdrometers, Geophys. Res. Lett., 37, doi:10.1029/2010GL044120, 2010.

Tapiador, F. J., Haddad, Z. S., and Turk, J.: A Probabilistic View on Raindrop Size Distribution Modeling: A Physical Interpretation of Rain Microphysics, J. Hydrometeor., 15, 427–443, doi:10.1175/JHM-D-13-033.1, 2014.

Tapiador, F. J., Navarro, A., Moreno, R., Jiménez-Alcázar, A., Marcos, C., Tokay, A., Durán, L., Bodoque, J. M., Martín, R., Petersen, W., and de Castro, M.: On the Optimal Measuring Area for Pointwise Rainfall Estimation: A Dedicated Experiment with 14 Laser Disdrometers, Journal of Hydrometeorology, 18, 753–760, doi:10.1175/JHM-D-16-0127.1, 2017.

Testud, J., Bouar, E. L., Obligis, E., and Ali-Mehenni, M.: The Rain Profiling Algorithm Applied to Polarimetric Weather Radar, J. Atmos. Oceanic Technol., 17, 332–356, doi:10.1175/1520-0426(2000)017<0332:TRPAAT>2.0.CO;2, 2000.

Thurai, M., Huang, G., Bringi, V., Randeu, W., and Schönhuber, M.: Drop shapes, model comparisons, and calculations of polarimetric radar parameters in rain, J. Atmos. Oceanic Technol., 24, 1019–1032, doi:10.1175/JTECH2051.1, 2007.

Thurai, M., Bringi, V. N., Szakáll, M., Mitra, S. K., Beard, K. V., and Borrmann, S.: Drop Shapes and Axis Ratio Distributions: Comparison between 2D Video Disdrometer and Wind-Tunnel Measurements, J. Atmos. Oceanic Technol., 26, 1427–1432, doi:10.1175/2009JTECHA1244.1, 2009.

Thurai, M., Petersen, W., Tokay, A., Schultz, C., and Gatlin, P.: Drop size distribution comparisons between Parsivel and 2-D video disdrometers, Adv. Geosci., 30, 3–9, doi:10.5194/adgeo-30-3-2011, 2011.

Thurai, M., Bringi, V., Carey, L., Gatlin, P., Schultz, E., and Petersen, W.: Estimating the accuracy of polarimetric radar-based retrievals of drop-size distribution parameters and rain rate: An application of error variance separation using radar-derived spatial correlations, Journal of Hydrometeorology, 13, 1066–1079, doi:10.1175/JHM-D-11-070.1, 2012.

Tokay, A., Wolff, D. B., and Petersen, W. A.: Evaluation of the New Version of the Laser-Optical Disdrometer, OTT Parsivel^2, J. Atmos. Oceanic Technol., 31, 1276–1288, doi:10.1175/JTECH-D-13-00174.1, 2014.

Tridon, F., Van Baelen, J., and Pointin, Y.: Aliasing in Micro Rain Radar data due to strong vertical winds, Geophys. Res. Lett., 38, L02804, doi:10.1029/2010GL046018, 2011.

Uijlenhoet, R., Steiner, M., and Smith, J. A.: Variability of raindrop size distributions in a squall line and implications for radar rainfall estimation, J. Hydrometeor., 44, 43–61, doi:10.1175/1525-7541(2003)004<0043:VORSDI>2.0.CO;2, 2003.

Ulbrich, C. W.: Natural variations in the analytical form of the raindrop-size distribution, J. Climate Appl. Meteor., 22, 1764–1775, doi:10.1175/1520-0450(1983)022<1764:NVITAF>2.0.CO;2, 1983.

Ulbrich, C. W.: The Effects of Drop Size Distribution Truncation on Rainfall Integral Parameters and Empirical Relations, J. Climate Appl. Meteor., 24, 580–590, doi:10.1175/1520-0450(1985)024<0580:TEODSD>2.0.CO;2, 1985.

Vivekanandan, J., Zhang, G., and Brandes, E.: Polarimetric radar estimators based on a constrained gamma drop size distribution model, J. Appl. Meteor., 43, 217–230, doi:10.1175/1520-0450(2004)043<0217:PREBOA>2.0.CO;2, 2004.

Vulpiani, G., Marzano, F. S., Chandrasekar, V., Berne, A., and Uijlenhoet, R.: Polarimetric weather radar retrieval of raindrop size distribution by means of a regularized artificial neural network, IEEE T. Geosci. Remote Sens., 44, 3262–3275, doi:10.1109/TGRS.2006.878438, 2006.

Willis, P. T.: Functional fits to some observed drop size distributions and parameterization of rain, J. Atmos. Sci., 41, 1648–1661, doi:10.1175/1520-0469(1984)041<1648:FFTSOD>2.0.CO;2, 1984.

Wolfensberger, D., Scipion, D., and Berne, A.: Detection and characterization of the melting layer based on polarimetric radar scans, Quarterly Journal of the Royal Meteorological Society, doi:10.1002/qj.2672, 2015.

Yoshikawa, E., Chandrasekar, V., and Ushio, T.: Raindrop Size Distribution (DSD) Retrieval for X-Band Dual-Polarization Radar, J. Atmos. Oceanic Technol., 31, 387–403, doi:10.1175/JTECH-D-12-00248.1, 2014.

Zhang, G., Vivekanandan, J., and Brandes, E.: A method for estimating rain rate and drop size distribution from polarimetric radar measurements, IEEE T. Geosci. Remote Sens., 39, 830–841, doi:10.1109/36.917906, 2001.

Zhang, G., Vivekanandan, J., Brandes, E. A., Meneghini, R., and Kozu, T.: The shape-slope relation in observed gamma raindrop size distributions: Statistical error or useful information?, Journal of Atmospheric and Oceanic Technology, 20, 1106–1119, doi:10.1175/1520-0426(2003)020<1106:TSRIOG>2.0.CO;2, 2003.

Table A1. Comparison of double-moment method to SCOP-ME results on all Parsivel data in the HyMeX data set by axis ratio function (Ratio). RB [%] is median relative bias, IQR [% pts] is interquartile range of relative bias [% points], r^2 is squared correlation coefficient. S is the slope on measured vs. reconstructed regression. Difference is difference in absolute values for RB and IQR, and difference in deviation from unity for r^2 and slope. A negative difference shows that the double-moment method improved on SCOP-ME's performance.

		Double-moment				SCOP-ME				Difference			
Ratio	Var	RB	IQR	r^2	S	RB	IQR	r^2	S	RB	IQR	r^2	S
Ands.	D_m	−1	10	0.85	0.99	−2	9	0.88	0.83	−1	1	0.04	−0.17
	M_0	20	80	0.70	0.97	13	70	0.66	0.98	7	10	−0.04	0.01
	M_1	10	52	0.79	0.97	12	50	0.80	1.09	−1	2	0.02	−0.06
	M_2	6	34	0.89	1.03	10	34	0.91	1.13	−4	−0	0.02	−0.10
	M_3	4	21	0.97	1.09	8	21	0.97	1.07	−4	0	0.00	0.02
	M_4	3	12	0.99	1.09	6	11	0.99	0.99	−3	1	0.00	0.08
	M_5	1	6	0.99	1.03	3	4	0.99	0.93	−2	2	0.00	−0.04
	M_6	0	3	0.98	0.94	2	3	0.98	0.89	−2	1	−0.01	−0.06
	M_7	−1	14	0.98	0.83	1	3	0.94	0.83	0	11	−0.04	0.00
	R	3	14	0.99	1.11	6	12	0.98	1.02	−3	2	0.00	0.09
Thur.	D_m	−1	13	0.83	0.99	−0	12	0.87	0.78	1	1	0.04	−0.21
	M_0	14	94	0.64	0.91	2	74	0.55	0.89	13	20	−0.09	−0.03
	M_1	7	64	0.75	0.94	1	55	0.73	1.05	6	9	−0.02	0.02
	M_2	4	42	0.88	1.02	1	39	0.88	1.15	3	3	0.00	−0.13
	M_3	4	26	0.96	1.09	1	26	0.96	1.14	3	1	0.00	−0.05
	M_4	3	14	0.99	1.09	1	14	0.99	1.06	2	0	0.00	0.03
	M_5	1	7	0.99	1.03	1	5	0.99	0.98	0	2	0.00	0.02
	M_6	0	2	0.99	0.94	2	2	0.98	0.92	−2	0	−0.01	−0.02
	M_7	−1	12	0.98	0.81	4	5	0.94	0.84	−3	7	−0.04	0.03
	R	3	16	0.99	1.12	1	16	0.99	1.09	2	0	0.00	0.02
Bran.	D_m	−0	11	0.83	0.99	1	10	0.87	0.80	−0	0	0.04	−0.18
	M_0	14	79	0.66	0.90	−3	66	0.58	0.86	11	13	−0.08	−0.04
	M_1	5	53	0.75	0.92	−3	48	0.75	1.00	3	5	−0.01	0.08
	M_2	2	35	0.87	1.02	−2	34	0.88	1.08	−1	1	0.01	−0.07
	M_3	0	23	0.96	1.10	−2	22	0.96	1.07	−1	1	0.00	0.03
	M_4	0	15	0.99	1.11	−1	12	0.99	1.00	−1	3	0.00	0.10
	M_5	−1	7	0.99	1.06	−0	4	0.99	0.94	0	3	0.00	−0.01
	M_6	0	3	0.98	0.98	2	3	0.98	0.89	−2	−0	−0.01	−0.08
	M_7	1	15	0.98	0.87	5	6	0.94	0.84	−5	9	−0.04	−0.03
	R	−0	17	0.98	1.12	−1	13	0.98	1.02	−1	4	0.00	0.10
Beard	D_m	−1	10	0.85	0.99	−1	10	0.88	0.80	−0	1	0.04	−0.19
	M_0	15	78	0.69	0.93	6	69	0.61	0.94	9	9	−0.08	0.02
	M_1	6	52	0.78	0.94	5	50	0.77	1.08	1	2	−0.01	−0.02
	M_2	3	34	0.89	1.03	4	34	0.90	1.16	−1	−0	0.01	−0.13
	M_3	2	22	0.97	1.10	4	21	0.97	1.13	−2	1	0.00	−0.02
	M_4	2	13	0.99	1.11	3	11	0.99	1.05	−1	3	0.00	0.07
	M_5	1	7	0.99	1.06	2	4	1.00	0.98	−1	4	0.01	0.03
	M_6	1	3	0.98	0.96	2	3	0.98	0.93	−1	−0	0.00	−0.03
	M_7	0	14	0.98	0.83	3	4	0.95	0.86	−2	10	−0.03	0.03
	R	2	15	0.99	1.13	3	12	0.99	1.08	−1	3	0.00	0.05

Table A2. Comparison of double-moment method to SCOP-ME results on all Parsivel data in the Payerne data set by axis ratio function (Ratio). Columns are as for Table A1.

		Double-moment				SCOP-ME				Difference			
Ratio	Var	RB	IQR	r^2	S	RB	IQR	r^2	S	RB	IQR	r^2	S
Ands.	D_m	1	8	0.85	1.15	−0	7	0.88	0.92	1	1	0.04	0.08
	M_0	10	63	0.60	0.88	−1	45	0.70	0.89	9	17	0.09	0.01
	M_1	2	40	0.74	0.89	1	35	0.80	0.96	1	5	0.06	0.07
	M_2	−0	25	0.87	0.94	3	25	0.89	0.99	−3	−0	0.02	0.05
	M_3	−0	14	0.96	1.00	4	16	0.95	0.98	−4	−2	−0.01	−0.01
	M_4	1	8	0.99	1.05	4	8	0.98	0.94	−3	−0	−0.01	−0.01
	M_5	1	4	0.99	1.05	3	3	0.98	0.84	−2	1	−0.01	−0.11
	M_6	0	2	0.98	0.93	2	2	0.96	0.71	−2	−0	−0.02	−0.22
	M_7	0	9	0.96	0.76	1	2	0.95	0.59	−1	7	−0.01	−0.17
	R	0	9	0.99	1.04	4	9	0.97	0.97	−4	−0	−0.01	0.01
Thur.	D_m	1	10	0.83	1.18	2	9	0.87	0.90	−1	2	0.04	0.08
	M_0	7	73	0.56	0.85	−11	46	0.66	0.82	−4	27	0.11	−0.03
	M_1	0	48	0.70	0.86	−8	36	0.78	0.90	−8	12	0.08	0.04
	M_2	−1	31	0.84	0.91	−6	27	0.88	0.95	−4	4	0.04	0.04
	M_3	−0	19	0.95	0.97	−3	18	0.95	0.97	−3	0	0.00	0.00
	M_4	1	10	0.99	1.03	−1	10	0.98	0.96	−0	−0	−0.01	−0.02
	M_5	1	4	0.99	1.03	0	4	0.98	0.87	1	0	−0.01	−0.10
	M_6	0	2	0.98	0.92	2	2	0.96	0.73	−2	−0	−0.02	−0.19
	M_7	−0	7	0.96	0.75	4	4	0.95	0.61	−4	3	−0.01	−0.15
	R	0	11	0.98	1.02	−1	12	0.98	0.98	−1	−1	0.00	0.00
Bran.	D_m	2	10	0.83	1.15	3	9	0.87	0.90	−1	1	0.04	0.05
	M_0	3	65	0.57	0.83	−14	44	0.66	0.80	−12	21	0.09	−0.03
	M_1	−3	44	0.72	0.86	−12	35	0.78	0.87	−8	10	0.06	0.02
	M_2	−4	29	0.85	0.92	−9	26	0.88	0.93	−4	3	0.03	0.01
	M_3	−3	18	0.95	1.00	−5	18	0.95	0.96	−3	0	0.00	−0.04
	M_4	−1	10	0.99	1.08	−3	10	0.98	0.94	−2	0	0.00	0.02
	M_5	−0	5	0.99	1.10	−0	4	0.98	0.87	−0	1	0.00	−0.03
	M_6	0	2	0.98	0.99	3	2	0.97	0.74	−2	−0	−0.01	−0.25
	M_7	1	9	0.96	0.82	6	4	0.96	0.63	−4	5	−0.01	−0.19
	R	−2	11	0.98	1.06	−3	11	0.98	0.96	−1	0	−0.01	0.02
Beard	D_m	1	9	0.84	1.14	1	8	0.88	0.89	0	1	0.04	0.03
	M_0	6	61	0.60	0.86	−7	45	0.68	0.87	−1	16	0.08	0.01
	M_1	−1	40	0.74	0.89	−5	34	0.80	0.95	−4	6	0.06	0.06
	M_2	−3	25	0.87	0.95	−2	25	0.89	1.00	0	1	0.03	0.05
	M_3	−2	16	0.96	1.02	−0	16	0.96	1.02	1	−0	0.00	0.00
	M_4	−0	10	0.99	1.07	1	9	0.99	0.99	−1	1	−0.01	0.06
	M_5	1	5	0.99	1.07	2	3	0.98	0.90	−1	2	0.00	−0.03
	M_6	1	2	0.98	0.94	2	2	0.97	0.75	−1	−0	−0.01	−0.19
	M_7	1	9	0.96	0.76	3	3	0.96	0.63	−2	6	0.00	−0.13
	R	−1	11	0.99	1.07	1	10	0.98	1.01	−0	1	0.00	0.05

Table A3. Comparison of double-moment method to SCOP-ME results on all Parsivel data in the Iowa data set by axis ratio function (Ratio). Columns are as for Table A1.

		Double-moment				SCOP-ME				Difference			
Ratio	Var	RB	IQR	r^2	S	RB	IQR	r^2	S	RB	IQR	r^2	S
Ands.	D_m	2	13	0.86	1.07	0	12	0.91	0.85	2	1	0.04	−0.08
	M_0	−11	72	0.53	0.61	−4	73	0.48	0.75	6	−1	−0.04	0.14
	M_1	−9	52	0.70	0.74	−2	54	0.75	1.03	7	−2	0.05	0.23
	M_2	−6	36	0.89	0.92	0	37	0.92	1.11	6	−1	0.03	−0.03
	M_3	−2	25	0.97	1.09	2	23	0.98	1.04	0	2	0.01	0.04
	M_4	1	17	0.99	1.14	2	12	1.00	0.97	−1	5	0.01	0.11
	M_5	0	8	0.99	1.08	1	5	0.99	0.91	−1	4	0.00	−0.02
	M_6	1	4	0.99	0.93	2	4	0.98	0.85	−1	0	−0.01	−0.08
	M_7	0	19	0.98	0.77	2	5	0.95	0.79	−2	14	−0.03	0.02
	R	1	19	0.99	1.16	2	14	0.99	1.00	−1	5	0.01	0.16
Thur.	D_m	2	15	0.86	1.10	1	13	0.90	0.83	1	2	0.04	−0.07
	M_0	−11	85	0.46	0.59	−9	78	0.39	0.69	2	7	−0.06	0.10
	M_1	−9	63	0.66	0.71	−6	59	0.70	1.03	3	4	0.05	0.26
	M_2	−4	44	0.88	0.88	−3	42	0.91	1.16	1	2	0.03	−0.04
	M_3	0	27	0.98	1.04	−1	27	0.98	1.10	−1	0	0.01	−0.06
	M_4	3	15	0.99	1.11	0	14	1.00	1.01	3	1	0.00	0.09
	M_5	2	7	0.99	1.05	0	5	0.99	0.93	1	2	0.00	−0.02
	M_6	1	3	0.99	0.92	2	3	0.97	0.86	−1	−0	−0.01	−0.06
	M_7	−1	14	0.98	0.77	3	6	0.95	0.80	−3	8	−0.03	0.02
	R	3	17	0.99	1.11	0	16	0.99	1.05	2	1	0.01	0.06
Bran.	D_m	2	14	0.86	1.10	1	12	0.90	0.86	0	1	0.04	−0.04
	M_0	−9	77	0.61	0.77	−10	71	0.56	0.82	−1	6	−0.05	0.05
	M_1	−8	56	0.71	0.76	−8	52	0.76	1.01	1	3	0.05	0.22
	M_2	−5	38	0.89	0.90	−5	37	0.92	1.08	0	1	0.03	0.02
	M_3	−2	25	0.97	1.08	−3	24	0.98	1.03	−1	1	0.01	0.05
	M_4	1	17	0.99	1.15	−2	12	1.00	0.96	−1	4	0.01	0.11
	M_5	0	8	0.99	1.10	−1	5	0.99	0.90	−1	3	0.00	0.01
	M_6	1	3	0.99	0.97	2	4	0.97	0.85	−1	−1	−0.01	−0.12
	M_7	1	17	0.98	0.82	4	8	0.95	0.80	−3	9	−0.04	−0.02
	R	−0	18	0.98	1.16	−2	14	0.99	0.99	−2	4	0.01	0.15
Beard	D_m	2	13	0.86	1.07	0	12	0.91	0.83	2	1	0.04	−0.10
	M_0	−9	76	0.52	0.62	−5	78	0.45	0.77	4	−3	−0.07	0.14
	M_1	−8	55	0.70	0.75	−2	58	0.73	1.08	6	−3	0.04	0.17
	M_2	−4	38	0.89	0.94	0	40	0.92	1.18	4	−2	0.02	−0.12
	M_3	−0	26	0.98	1.09	2	25	0.98	1.11	−2	1	0.00	−0.01
	M_4	3	18	0.99	1.14	2	13	1.00	1.01	0	6	0.00	0.13
	M_5	1	9	0.99	1.08	2	4	0.99	0.93	−0	5	0.00	0.00
	M_6	1	3	0.99	0.94	2	3	0.97	0.86	−1	−0	−0.02	−0.08
	M_7	0	18	0.98	0.78	3	5	0.95	0.79	−2	13	−0.03	0.01
	R	2	20	0.99	1.16	2	15	0.99	1.06	−0	6	0.00	0.11

Table A4. Differences in performance by variable and region, for DSDs retrieved from noise-corrected PPI data using the double-moment technique and SCOP-ME, compared to the MRR at Pradel Grainage (MRR) and Parsivels by region (HyMeX, Payerne, and Iowa). Metrics and differences are defined as for Table A1. An exception is Z, which refers to Z_H measured by the radar, not reconstructed through DSD-retrieval (hence it is the same for both techniques).

		Double-moment				SCOP-ME				Difference			
	Variable	RB	IQR	r^2	S	RB	IQR	r^2	S	RB	IQR	r^2	S
MRR	D_m	−7	26	0.28	0.42	−6	26	0.31	0.43	1	−1	0.03	0.01
	M_0	26	181	0.00	0.01	17	160	0.00	0.01	9	21	0.00	0.00
	M_1	21	156	0.01	0.02	24	149	0.01	0.02	−3	7	0.00	0.00
	M_2	19	133	0.01	0.05	27	134	0.01	0.04	−7	−1	0.00	0.00
	M_3	11	107	0.02	0.12	22	113	0.01	0.11	−11	−5	−0.01	0.00
	M_4	−1	88	0.04	0.44	12	99	0.03	0.41	−11	−11	−0.01	−0.03
	M_5	−8	74	0.13	1.79	3	83	0.11	1.56	6	−9	−0.02	0.23
	M_6	−15	78	0.26	3.61	−12	82	0.18	2.97	3	−4	−0.08	0.64
	M_7	−19	91	0.29	4.07	−26	88	0.18	3.21	−7	3	−0.11	0.86
	R	2	94	0.03	0.27	17	106	0.03	0.26	−15	−12	0.00	−0.01
	Z	−3	16	0.63	0.89	−3	16	0.63	0.89	0	0	0.00	0.00
HyMeX	D_m	−6	26	0.29	0.50	−5	25	0.31	0.43	1	1	0.02	−0.07
	M_0	−3	150	0.02	0.28	−10	120	0.04	0.26	−7	30	0.02	−0.02
	M_1	−10	122	0.04	0.36	−13	110	0.07	0.35	−3	12	0.03	−0.01
	M_2	−14	104	0.11	0.46	−16	100	0.13	0.45	−2	4	0.02	−0.01
	M_3	−20	95	0.21	0.49	−21	93	0.21	0.48	−2	1	0.00	−0.01
	M_4	−26	94	0.22	0.41	−26	93	0.24	0.41	−1	1	0.02	0.00
	M_5	−32	96	0.13	0.30	−32	96	0.19	0.31	0	−0	0.06	0.01
	M_6	−39	100	0.05	0.21	−37	105	0.11	0.22	2	−6	0.06	0.01
	M_7	−46	106	0.02	0.16	−41	118	0.06	0.17	5	−12	0.04	0.01
	R	−21	97	0.24	0.47	−22	96	0.23	0.46	−1	2	−0.01	−0.01
	Z	−9	26	0.50	0.68	−9	26	0.50	0.68	0	0	0.00	0.00
Payerne	D_m	−7	22	0.21	0.34	−5	22	0.21	0.30	2	−0	0.00	−0.03
	M_0	31	171	0.07	0.50	−4	124	0.11	0.34	27	47	0.04	−0.16
	M_1	17	138	0.08	0.43	−1	121	0.11	0.36	16	17	0.03	−0.08
	M_2	6	119	0.12	0.43	−1	114	0.14	0.40	5	5	0.02	−0.03
	M_3	−4	106	0.19	0.46	−5	105	0.20	0.46	−2	2	0.01	−0.01
	M_4	−13	99	0.29	0.48	−12	99	0.27	0.50	1	0	−0.02	0.01
	M_5	−22	103	0.29	0.37	−21	104	0.26	0.41	1	−1	−0.03	0.04
	M_6	−31	107	0.12	0.12	−29	110	0.11	0.15	2	−3	−0.01	0.02
	M_7	−42	109	0.03	0.02	−40	116	0.02	0.03	2	−8	−0.01	0.01
	R	−7	108	0.26	0.51	−6	107	0.25	0.51	1	1	−0.01	0.01
	Z	−8	28	0.42	0.57	−8	28	0.42	0.57	0	0	0.00	0.00
Iowa	D_m	−10	28	0.33	0.39	−11	26	0.37	0.34	−1	1	0.04	−0.04
	M_0	8	111	0.08	0.72	26	129	0.09	0.56	−18	−18	0.01	−0.16
	M_1	7	100	0.14	0.79	19	118	0.14	0.67	−12	−18	0.00	−0.13
	M_2	6	109	0.22	0.75	11	114	0.22	0.68	−5	−5	0.00	−0.08
	M_3	4	106	0.31	0.59	4	105	0.30	0.56	−0	1	−0.01	−0.02
	M_4	−5	107	0.33	0.37	−6	105	0.32	0.39	−1	2	−0.01	0.02
	M_5	−17	109	0.25	0.19	−15	110	0.28	0.23	2	−1	0.03	0.04
	M_6	−32	116	0.13	0.08	−25	123	0.18	0.12	7	−7	0.05	0.03
	M_7	−44	114	0.04	0.03	−35	135	0.09	0.06	10	−21	0.05	0.02
	R	4	113	0.33	0.49	2	109	0.32	0.50	3	4	−0.01	0.01
	Z	−5	25	0.54	0.62	−5	25	0.54	0.62	0	0	0.00	0.00